ESD-TR-66-566

4

Solid State Research

1966

Prepared under Electronic Systems Division Contract AF 19(628)-5167 by

Lincoln Laboratory

MASSACHUSETTS INSTITUTE OF TECHNOLOGY

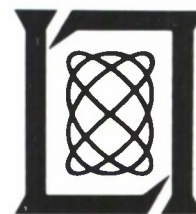Lexington, Massachusetts

AD647688

4

Solid State Research

1966

Lincoln Laboratory

MASSACHUSETTS INSTITUTE OF TECHNOLOGY

Lexington, Massachusetts

ABSTRACT

This report covers in detail the solid state research work at Lincoln Laboratory for the period 1 August through 31 October 1966. The topics covered are Solid State Device Research, Optical Techniques and Devices, Materials Research, and Physics of Solids.

INTRODUCTION

I. SOLID STATE DEVICE RESEARCH

Photovoltaic response has been observed in p-n junctions of $Pb_{1-x}Sn_xTe$ at wavelengths up to 11μ at $77°K$ and 14μ at $12°K$. Noise measurements at $12°K$ give a noise equivalent power for a $Pb_{0.86}Sn_{0.14}Te$ diode of about $5 \times 10^{-12}\,W\,sec^{1/2}$ and a D^* of $8 \times 10^9\,cm/W\,sec^{1/2}$ at 11μ. The responsivity cutoff of a $Pb_{0.83}Sn_{0.17}Te$ diode, taken at 50 percent of the peak responsivity, is 14μ at $12°K$ and 11μ at $77°K$. These results indicate that alloys in this series have considerable potential for infrared detection throughout the 8- to 14-μ atmospheric window and well beyond.

Infrared laser emission has been observed at $12°K$ and $77°K$ from diodes of $Pb_{1-y}Sn_ySe$ and $Pb_{1-x}Sn_xTe$. A $Pb_{1-x}Sn_xSe$ diode with a nominal Sn composition of .5 percent produced laser emission at 12.4μ at $12°K$ and at 10.2μ at $77°K$. Spontaneous emission from different $Pb_{1-x}Sn_xTe$ diodes at $12°K$ was observed at 9.4, 12.7, 13.5 and 13.7μ. The third diode in this series also produced laser emission at 10.6μ at $77°K$.

The Interface-alloy technique has been used to produce heterojunctions between GaAs and InSb. Despite the relatively large 14 percent lattice mismatch between the semiconductors, these heterojunctions are single-crystal, with an interdiffusion of the four elements of less than $2\,\mu$. Photocurrent, current-voltage and capacitance-voltage measurements are explained by a model for the heterojunction band structure employing a linearly-graded energy gap of the order of $60\overset{\circ}{A}$ long joining the GaAs to the InSb.

A 400 keV Van de Graaff positive ion accelerator has been used to implant phosphorus ions in germanium. Experimental evidence indicates that the implanted ions have produced n-type regions in bulk p-type material. Implantation for one hour with an incident phosphorus beam current of $0.4\,\mu A$ resulted in a phosphorus concentration at the sample surface of the order of $1 \times 10^{20}\,cm^{-3}$, and an n-type region approximately $2\,\mu$ deep.

By taking the negative mobility as an adjustable parameter, we have obtained good quantitative agreement between the measured small-signal admittance parameters of GaAs negative conductance amplifiers and those calculated from the three-slope piecewise-linear model for velocity vs electric field. The same set of parameter values also provides both a reasonable fit to the measured current-voltage characteristics and a correct prediction of the frequency and threshold bias for oscillation.

Very pure epitaxial layers of GaAs have been grown on Cr-doped semi-insulating GaAs substrates. The best layers have electron concentrations in the high 10^{14} to low $10^{15}\,cm^{-3}$ range, both at room temperature and at $77°K$. The electron mobilities for these layers are typically $8000\,cm^2/V\,sec$ at room temperature, and increase at $77°K$ to values as high as $77,000\,cm^2/V\,sec$. Gunn effect oscillators made from similar films deposited on heavily doped substrates have yielded power conversion efficiencies as high as 9 percent from devices delivering a peak output power of 1.75 watts at 9.3 GHz. This represents a substantial

improvement over previously reported results of other workers and demonstrates that Gunn oscillators with relatively high efficiencies can be fabricated using epitaxially grown GaAs.

II. OPTICAL TECHNIQUES AND DEVICES

Heterodyne sensitivity at 10.6 μm has been measured using a Cu-doped germanium photoconductor at liquid helium temperature. The measured minimum detectable power is within 10 dB of the theoretical limit, $h\nu B = 2 \times 10^{-20}$ W/Hz bandwidth. The signal frequency was 60 kHz and the noise bandwidth approximately 300 kHz.

A sealed-off CO_2 laser has been operated for approximately 100 hours without serious loss in output power. Although the gas fill was CO_2, N_2 and He, spectra of the visible spontaneous emission from the side of the tube indicate the presence of CO, CN, and N_2. The mechanism of formation of the additional constituents is being investigated to determine their relation to the operating life limitations of sealed-off systems.

III. MATERIALS RESEARCH

The crystal structure of Nd_2O_2Te has been determined by computer analysis of x-ray powder diffraction data. The atomic arrangement is derived from the K_2NiF_4 structure, in which the rare earth atoms exhibit an unusual nine-fold coordination.

In order to determine the cause of the anomaly observed in the x-ray scattering of ZnSe, neutron diffraction measurements have been made on this compound at room temperature and liquid helium temperature. The results obtained so far are inconclusive because of difficulties in evaluating background intensity corrections.

The phase diagram of Ag_2Te at high pressure has been investigated by means of electrical resistivity and x-ray diffraction measurements. Evidence has been obtained for three high-pressure phases, two of which exist at room temperature.

Hysteresis of the first-order $B8_1 \rightleftarrows B31$ magnetic transition in MnAs has been studied by measuring the resistivity and magnetic susceptibility as functions of pressure and temperature. The experimental results, together with earlier data for $MnAs_{1-x}P_x$, show that the transition is due to a large exchange striction in the basal planes together with a volume-dependent Weiss molecular field and manganese atomic moment.

The retrograde solubility of Pb in PbS has been investigated by means of Hall coefficient measurements on n-type samples prepared by annealing and quenching single crystals containing excess Pb. The carrier concentration decreases with decreasing annealing temperature from 2.4×10^{19} cm^{-3} for 912°C to 1.3×10^{18} cm^{-3} for 350°C.

Measurements of the Hall coefficient vs temperature for S-doped GaSb have shown that the lowest donor level of sulfur lies about 0.075 eV below the lowest conduction band at atmospheric pressure. The pressure dependence of resistivity at room temperature shows that this donor level is associated primarily with the conduction band minima at the (100) zone faces.

The magnetoresistance and Hall coefficient of high-purity and V-doped Ti_2O_3 single crystals have been measured at magnetic fields up to 218 kG. The high magnetoresistance of the high-purity samples at 4.2°K is inconsistent with a conventional one-band carrier transport mechanism. The p-type conductivity and negative magnetoresistance of V-doped Ti_2O_3 suggest that part of the V is present in the quadrivalent state.

Efficient pulsed laser operation has been obtained in Nd-doped YVO_4 single crystals. The threshold is only about 1 joule. This low threshold is due to the reduced Stark splitting of Nd^{+3} ions in YVO_4 and to substantial transfer of absorbed energy from the lattice to the Nd^{+3} ions.

A method employing PbTe and SnTe as standards has been developed for determining the presence of Pb and Sn in $Pb_{1-x}Sn_xTe$ alloys by electron microprobe analysis. The results are in good agreement with those obtained by wet chemical techniques.

IV. PHYSICS OF SOLIDS

The optical study of metals and semiconductors by means of sensitive differential techniques is continuing. One of these methods, the current pulse modulation technique, has been applied to the study of gold and nickel in the energy region from 2 to 10 eV; much well defined structure not observed in the standard reflectivity has been found. This same modulation technique is also being used in InSb to study the magneto-oscillations associated with transitions across the direct energy band gap, and also from the spin-orbit split-off valence band to the $\vec{k} = 0$ conduction band.

Oscillations in the infrared magnetoreflectivity of arsenic have been observed for the first time. Two distinct sets of interband transitions, taking place at different points in the Brillouin zone, have been seen.

The optical study of the effects of calibrated uniaxial stress on infrared transitions in S-doped silicon continues. A value for the pure shear deformation potential of the conduction band, $E_2 = 7.9$ eV, is obtained from the behavior of the p-like transitions. The application of stress helps distinguish between possible symmetries of observed centers, and aids in identification.

While studying polaron effects in InSb, a discontinuity in the functional dependence of the polaron cyclotron energy on magnetic field was observed near the LO phonon energy; this phenomenon had been predicted theoretically. In addition, absorption lines associated with donor states were found to exhibit polaron effects.

Experiments, in collaboration with Professor W. Paul's group at Harvard, to establish the band ordering in the mercury chalcogenides have now been extended to studies of the pressure dependence of the absorption edge. These new experiments suggest the same relative energy level orderings at $\vec{k} = 0$ for the Γ_6 and Γ_8 bands in HgSe and HgTe, which is inconsistent with the previous conclusion derived from the pressure dependence of the thermoelectric power. This contradiction appears to have been resolved by Hall measurements under pressure which, although incomplete, indicate that at least some of the HgSe samples were not extrinsic, thereby invalidating the thermoelectric power interpretation.

An analysis is being made of the beating effects observed by Whitsett in Shubnikov-de Haas measurements in n-type HgSe. Using the theoretical energy momentum expressions derived by Kane for zinc blende materials with small energy gaps, an attempt is being made to construct the Fermi surface for this semiconductor.

The conductivity tensor in bismuth has been calculated, assuming an anisotropic effective mass for holes and the two-band model for the electrons. A detailed lineshape calculation for the magnetoreflection is now under way.

The electronic energy bands in silicon have been calculated by using the Fourier expansion technique in which the band parameters are determined from the experimental values for the energy gaps and effective masses. This band structure has allowed the calculation of a frequency dependent dielectric constant which is in reasonably good agreement with experiment.

Calculations using high temperature expansion techniques for an ensemble of spins interacting with a Heisenberg exchange interaction are continuing. Thermodynamic functions, such as the spin correlation function and zero field susceptibility, are being treated for any range of exchange interaction and any lattice. Higher order coefficients of the high temperature series for the zero field susceptibility have been incorporated in the arguments for phase transitions in two-dimensional Heisenberg models.

The study, in the time dependent Hartree-Fock approximation, of spin sound (or spin density waves) in unmagnetized or weakly magnetized Fermi gases has been concluded; the results will appear in the Physical Review. As a sequel to this work, the properties of ordinary density waves have been studied in the same approximation. In addition to the usual plasmon dispersion relation, another branch of the density oscillation spectrum is discussed.

In studying the influence of the electron-electron interaction on the transport properties of the conduction electrons in a metal, a model of an interacting electron gas driven by an external electromagnetic field and scattered by randomly distributed impurities has been considered; the electron-electron interaction is treated in the random phase approximation. So far this theory has been applied to the special case of a homogeneous electron gas in the Born approximation.

For the case of a Landau quasi-particle distribution function in the presence of random impurities, the transport theory is incomplete since it is only valid for $\omega = 0$ or $\omega\tau << 1$; for $\omega\tau >> 1$, the case of experimental interest, the result is incorrect. The possibility of a new approach, valid for an arbitrary ω is now being investigated.

Further results on stimulated scattering experiments in quartz at 2.1°K have lent additional support to the contention that the anomalous Brillouin shifts reported by Krivokhizha et al. were misinterpreted and are actually due to intense Raman radiation which sets in at low temperatures. This phase of the experiment is now completed; results have been submitted to Science.

A study of the effect of orientational correlation and molecular fields in second harmonic light scattering from liquids and gases, with application to temperature dependence and depolarization, has been concluded. The results are being prepared for publication.

Work on infrared Raman scattering in solids continues. Raman spectra have been observed in GaS, GaSe and trigonal selenium.

The analysis of a maser model of interstellar OH microwave emission has been published in Physical Review Letters. Further calculations of self-consistent populations under directional UV pumping and the effect of microwave saturation on mode suppression are now being carried out.

CONTENTS

Contents

ORGANIZATION

SOLID STATE DIVISION

A. L. McWhorter, *Head*
P. E. Tannenwald, *Associate Head*
M. J. Hudson, *Assistant*
E. P. Warekois
D. T. Stevenson*

SOLID STATE THEORY

II. J. Zeiger, *Leader*
M. M. Litvak, *Assistant Leader*

Argyres, P. N.	Larsen, D. M.
Chinn, S. R.†	Melanson, G. S., Jr.
Dresselhaus, G. F.	Palm, B. J.*
Kaplan, T. A.	Stanley, II. E.*
Kelley, P. L.	Trent, P. H.
Kleiner, W. II.	Van Zandt, L. L.

OPTICS AND INFRARED

R. II. Kingston, *Leader*
R. J. Keyes, *Assistant Leader*

Bates, D. II.	Longaker, P. R.
Bostick, II. A.	McPhie, J. M.
Carbone, R. J.	Quist, T. M.
Dennis, J. II.	Teich, M. C.
Freed, C.	Zimmerman, M. D.

ELECTRONIC MATERIALS

J. B. Goodenough, *Leader*
J. M. Honig, *Associate Leader*
A. J. Strauss, *Assistant Leader*

Anderson, C. H., Jr.	Iseler, G. W.
Andrews, II. I.†	Kafalas, J. A.
Arnott, R. J.	LaFleur, W. J.
Banus, M. D.	Lavine, M. C.*
Batson, D.	Longo, J. M.
Brebrick, R. F., Jr.	O'Connor, J. R.
Button, M. J.	Owens, E. B.
Delaney, E. J.	Plonko, M. C.
Ehlers, II. II.	Pollard, E. R.†
England, R. E.	Raccah, P. M.
Fahey, R. E.	Reed, T. B.
Farrell, L. B.	Roddy, J. T.
Ferretti, A.	Sohn, J. B.
Finn, M. C.	Soracco, D. J.
Hilsenrath, S.	Steininger, J. A.

SOLID STATE PHYSICS

J. G. Mavroides, *Leader*
G. B. Wright, *Assistant Leader*

Burke, J. W.	Mastromattei, E. L.
Carman, R. L.*	Menyuk, N.
Dickey, D. II.	Murphy, H. C.
Dresselhaus, M. S.	Nill, K. W.
Dwight, K., Jr.	Parker, C. D.
Feinleib, J.	Perry, F. II.
Feldman, B.	Scouler, W. J.
Fulton, M. J.	Stickler, J. J.†
Groves, S. II.	Strahm, N. D.†
Johnson, E. J.	Thaxter, J. B.
Kernan, W. C.	Weber, R.
Kolesar, D. F.	Weinberg, D. L.
Krag, W. E.	

APPLIED PHYSICS

J. O. Dimmock, *Leader*
T. C. Harman, *Assistant Leader*
I. Melngailis, *Assistant Leader*

Butler, J. F.	Foyt, A. G.	Mooradian, A.	Stella, J. A.
Calawa, A. R.	Halpern, J.	Oliver, M.†	Sullivan, F. M.
Carter, F. B.	Hinkley, E. D.	Paladino, A. E.	Ward, J. II. R., III
Caswell, F. H.	Hurwitz, C. E.	Palermo, J. S.	Wolfe, C. M.
Clough, T. F.	Lindley, W. T.	Phelan, R. J., Jr.	Youtz, P.
Donaldson, P. L.			

---

* Part Time

† Research Assistant

xiii

REPORTS BY AUTHORS
ENGAGED IN SOLID STATE RESEARCH

15 August through 15 November 1966

PUBLISHED REPORTS

Journal Articles*

JA No.

2620	A Volumetric Determination of Arsenic and Antimony in Mixed Manganese Arsenide, Antimonide and Phosphide Compounds	E. R. Whipple D. H. Ridgley	Anal. Chim. Acta $\underline{35}$, 499 (1966)
2719	Partial Pressures of $Te_2(g)$ in Equilibrium with $Ge_{1/2-\delta}Te_{1/2+\delta}(c)$ from Optical Density Data	R. F. Brebrick	J. Phys. Chem. Solids $\underline{27}$, 1495 (1966)
2723	Single Crystal Growth and Electrical Transport Properties of Intermediates in the Spinel System $CO_{1+\delta}V_{2-\delta}O_4$	D. B. Rogers A. Ferretti W. Kunnmann[†]	J. Phys. Chem. Solids $\underline{27}$, 1445 (1966)
2725A	Thermodynamic Aspects of the Temperature-Pressure Phase Diagram of InTe	M. D. Banus P. M. Robinson[†]	J. Appl. Phys. $\underline{37}$, 3771 (1966)
2727	Photoelectron Statistics Produced by a Laser Operating Below and Above the Threshold of Oscillation	C. Freed H. A. Haus[†]	IEEE J. Quant. Electron $\underline{QE-2}$, 190 (1966)
2739	Oscillatory Faraday Rotation of the Indirect Transition in Germanium at $1.7°K$	J. Halpern	J. Phys. Chem. Solids $\underline{27}$, 1505 (1966)
2740	Phonon Generation, Propagation, and Attenuation at 70 GHz	J. B. Thaxter P. E. Tannenwald	IEEE Trans. Sonics and Ultrasonics $\underline{SU-13}$, 61 (1966)
2768	Anomaly in the X-Ray Scattering of ZnSe	P. M. Raccah R. J. Arnott A. Wold[†]	Phys. Rev. $\underline{148}$, 904 (1966)
2774	Generalization of the Ruderman-Kittel-Kasuya-Yosida Interaction for Nonspherical Fermi Surfaces	L. M. Roth[†] H. J. Zeiger T. A. Kaplan	Phys. Rev. $\underline{149}$, 519 (1966)
2824	Incoherent Source Optical Pumping of Visible and Infrared Semiconductor Lasers	R. J. Phelan, Jr.	Proc. IEEE (Correspondence) $\underline{54}$, 1119 (1966)

---

* Reprints available.

† Author not at Lincoln Laboratory.

JA No.

2827	Efficient Ultraviolet Laser Emission in Electron-Beam-Excited ZnS	C.E. Hurwitz	Appl. Phys. Letters $\underline{9}$, 116 (1966)
2832	First Order Raman Effect in III-V Compounds	A. Mooradian G.B. Wright	Solid State Commun. $\underline{4}$, 431 (1966)
2847	Maser Model for Interstellar OH Microwave Emission	M.M. Litvak A.L. McWhorter M.L. Meeks H.J. Zeiger	Phys. Rev. Letters $\underline{17}$, 821 (1966)
2852	High Pressure Synthesis of Arsenopyrite-Type Ternary Compounds	M.D. Banus M.C. Lavine	Materials Res. Bull. $\underline{1}$, 3 (1966)
2853	Possibility of a Phase Transition for the Two-Dimensional Heisenberg Model	H.E. Stanley T.A. Kaplan	Phys. Rev. Letters $\underline{17}$, 913 (1966)
2869	Infrared Magnetoelectroreflectance in Ge, GaSb, and InSb	S.H. Groves C.R. Pidgeon* J. Feinleib	Phys. Rev. Letters $\underline{17}$, 643 (1966)
2894	Bulk GaAs Negative Conductance Amplifiers	A.L. McWhorter A.G. Foyt	Appl. Phys. Letters $\underline{9}$, 300 (1966)
2897	Photovoltaic Effect in $Pb_xSn_{1-x}Te$ Diodes	I. Melngailis A.R. Calawa	Appl. Phys. Letters $\underline{9}$, 304 (1966)
MS-1719	Maser Emission at 18 cm from Interstellar OH	M.M. Litvak A.L. McWhorter M.L. Meeks H.J. Zeiger	NEREM Record $\underline{8}$, 188 (1966)

*   *   *   *   *

UNPUBLISHED REPORTS

Journal Articles

JA No.

2652	Electron Recombination in Laser-Produced Hydrogen Plasma	M.M. Litvak D.F. Edwards	Accepted by J. Appl. Phys.
2796	Experimental Atomic Form-Factors in MgO	P.M. Raccah R.J. Arnott	Accepted by Phys. Rev.
2805	Spin Waves in Paramagnetic Fermi Gases	L.L. Van Zandt	Accepted by Phys. Rev.

---

* Author not at Lincoln Laboratory.

* Author not at Lincoln Laboratory.

MS No.

1702	Optical and Laser Properties of Nd^{+3}- and Eu^{+3}-Doped YVO_4	J.R. O'Connor	Accepted by Trans. Met. Soc. AIME
1771	Characterization of d Electrons in Solids by Structure	J.B. Goodenough	Accepted by Materials Res. Bull.

Meeting Speeches*

MS No.

1608	Oscillatory Magnetoabsorption of the Direct Transition in the Layer Compound GaSe at 1.5°K	J. Halpern	
1609	Polaron Induced Anomalies in InSb	D.M. Larsen E.J. Johnson	
1610	Sulfur Donors in Silicon: Infrared Transitions and the Effects of Calibrated Uniaxial Stress	W.E. Krag W.H. Kleiner H.J. Zeiger S. Fischler	International Conference on the Physics of Semiconductors, Kyoto, Japan, 8-13 September 1966
1611	Magneto-Piezo-Optical Experiments in Semiconductors	J.G. Mavroides M.S. Dresselhaus R.L. Aggerwal† G.F. Dresselhaus	
1612	Electron-Phonon Interaction in n-InSb at 9 GHz	K.W. Nill A.L. McWhorter	
1629A	Narrow Band Electrons in Transition-Metal Oxides	J.B. Goodenough	International Conference on Magnetic Oxides, Liblice, Czechoslovakia, 3-7 October 1966
1630	The Luminescence in a Magnetic Field of Excitons with a Screened Coulomb Potential	G.B. Wright	International Conference on Luminescence, Budapest, Hungary, 23-30 August 1966
1635	Injection Luminescence and Laser Action in Semiconductors	R.H. Rediker	
1681	Role of Spark Source Mass Spectroscopy	E.B. Owens	American Chemical Society, New York, 11-16 September 1966
1702	Optical and Laser Properties of Nd^{+3}- and Eu^{+3}-Doped YVO_4	J.R. O'Connor	Metallurgical Society of AIME Conference, Boston, 29-31 August 1966
1770	Recent Developments in Solid State Microwave Oscillators	A.L. McWhorter	

---

* Titles of Meeting Speeches are listed for information only. No copies are available for distribution.

† Author not at Lincoln Laboratory.

Reports

1715	Current Research Activities of the Solid State Physics Group at Lincoln Laboratory	G.B. Wright	Institute of Physics, Polish Academy of Sciences, Warsaw, 31 August 1966; Institute of Solid State Physics, Czechoslovak Academy of Sciences, Prague, 1 September 1966
1719A	Interstellar Maser Emission at 18 cm from OH Molecules	H.J. Zeiger	Optical and Infrared Laser Seminar, M.I.T., 28 October 1966
1719B	Interstellar OH Maser Emission	M.M. Litvak	Colloquium, Brandeis University, 8 November 1966
1726	Electron Beam Pumped Semiconductor Lasers	C.E. Hurwitz	NEREM, Boston, 2-4 November 1966
1772	Low-Energy-Gap Semiconducting Alloys for Infrared Emission and Detection	A.J. Strauss	Seminar, Texas Instruments, Inc., Dallas, Texas, 25 August 1966
1776	Coherent Infrared Radar	R.H. Kingston	IEEE Microwave Theory and Techniques and Electron Devices Joint Meeting, Boston, 18 October 1966
1784	Epitaxial GaAs Gunn Effect Oscillators	A.G. Foyt C.M. Wolfe	GaAs Symposium, University of Reading, England, 26-28 September 1966
1787	Spin Waves in Paramagnetic Fermi Gases	L.L. Van Zandt	Seminar, Ford Motor Scientific Research Laboratory, Dearborn, Michigan, 21 September 1966
1790	Retrograde Solubility in n-Type PbS	A.J. Strauss	Conference on Defects in Semiconductors, AIME, Chicago, Illinois, 31 October 1966
1806	Photovoltaic Effects in $Pb_xSn_{1-x}Te$ Diodes	I. Melngailis A.R. Calawa J.F. Butler T.C. Harman J.O. Dimmock	International Electron Devices Meeting, Washington, D.C., 26-28 October 1966
1813	Optimum Detection of CO_2 Laser Radiation by the Heterodyne Technique	M.C. Teich	Seminar, Cornell University, 11 November 1966

I. SOLID STATE DEVICE RESEARCH

A. PHOTOVOLTAIC EFFECT IN $Pb_{1-x}Sn_xTe$ DIODES

We have observed photovoltaic response in p-n junctions of $Pb_{1-x}Sn_xTe$ at wavelengths up to 11 μ at 77°K and 14 μ at 12°K. These results, together with previous photoluminescence data and the proposed model for the band structure of $Pb_{1-x}Sn_xTe$ (Ref. 1), indicate that these alloys have considerable potential for efficient infrared detection throughout the 8 to 14 μ atmospheric window and well beyond.

The results reported here were obtained with p-n junctions which formed in the vapor deposition process used in growing the alloys. Subsequently, junctions were also prepared by a diffusion technique previously used in fabricating PbTe diode lasers.[2] The alloy crystals had carrier concentrations in the range of 2 to 5×10^{17} cm^{-3} and mobilities in excess of 10^4 cm^2/ V sec at 77°K. Figures I-1(a) and -1(b) show current-voltage characteristics of a $Pb_{0.91}Sn_{0.09}Te$ and of a $Pb_{0.86}Sn_{0.14}Te$ diode respectively, at 12°K. These diodes were in the form of rectangular parallelepipeds with cleaved surfaces normal to the plane of the junction. The samples were mounted on a copper heat sink with the p-type layer attached to the copper. The thin n-type layer (< 20 μ) was exposed to the signal light. Liquid solder was used for making contacts in order to avoid heating the sample. In these early diodes no effort was made to treat the surface by etching. The reverse current in Figs. I-1(a) and -1(b) is thought to be mostly due to surface leakage. At 77°K the reverse current in these diodes was somewhat higher than at 12°K.

(a) $Pb_{0.91}Sn_{0.09}Te$ diode with area of 0.33×0.20 mm^2.

(b) $Pb_{0.86}Sn_{0.14}Te$ diode with area of 0.28×0.58 mm^2.
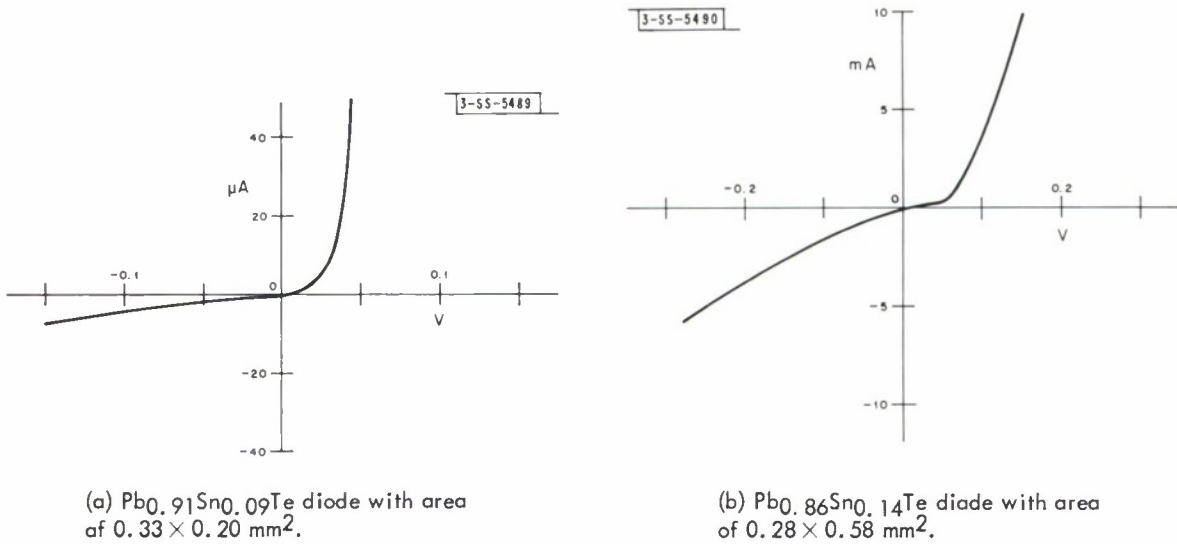
Fig. I-1. Current voltage characteristics at 12°K.

1
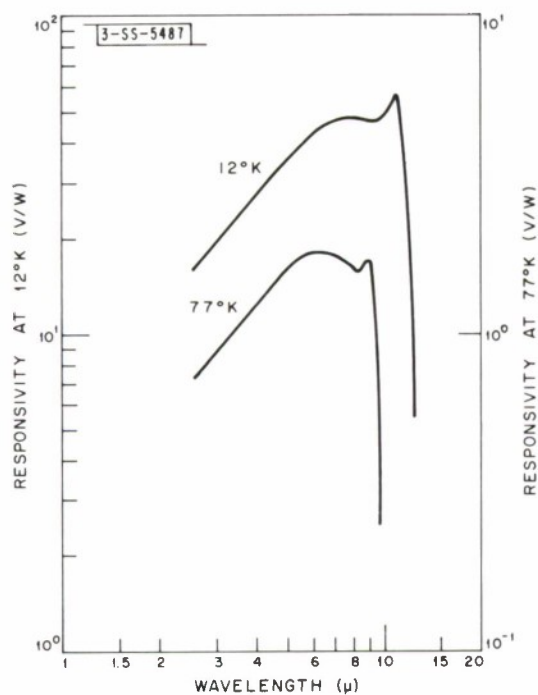
Fig. I-2. Responsivity spectro of $Pb_{0.86}Sn_{0.14}Te$ diode of Fig. I-1(b) at 12°K and ot 77°K.
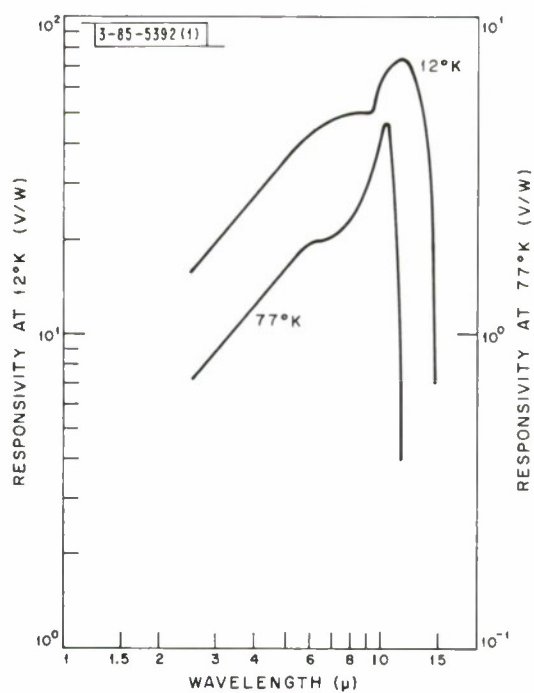
Fig. I-3. Responsivity spectra of $Pb_{0.83}Sn_{0.17}Te$ diode ot 12°K and ot 77°K.
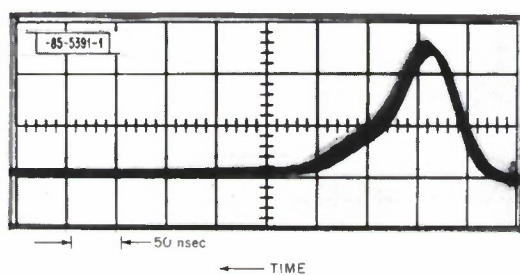
Fig. I-4. Response of $Pb_{0.83}Sn_{0.17}Te$ diode ot 77°K to o Q-switched CO_2 loser pulse.
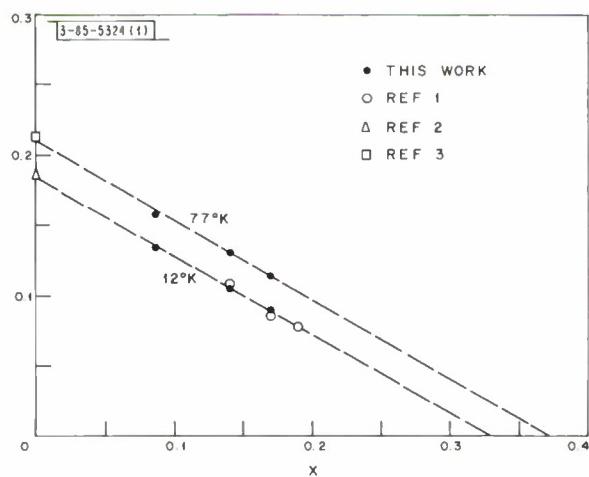
Fig. I-5. Energy gop of $Pb_{1-x}Sn_xTe$ os o function of mole froction of SnTe, x. The doto points ore obtoined from the cutoff of the photovoltoic responsivity (this work) ond from luminescence spectro.

Figure I-2 shows the spectral dependence of the open-circuit responsivity obtained with the $Pb_{0.86}Sn_{0.14}Te$ diode at zero bias. The responsivity at 12°K has a value of 57 V/W at 11 μ and at 77°K a value of 1.7 V/W at 9 μ. The enhancement observed in Fig. I-2 at both temperatures just prior to the long-wavelength cutoff can be attributed to an increase of carrier density at the junction as the radiation begins to penetrate the n-type layer in the vicinity of the bandgap absorption edge of the crystal. For wavelengths shorter than 5 μ, the responsivity at both temperatures has a slope slightly greater than unity, the slope expected for an ideal photon detector.

The number of carriers reaching the p-n junction per photon incident on the surface of the n-type layer has been estimated to be 0.1 at 12°K for the 11 μ wavelength. This estimate was based on a measurement of the short-circuit photocurrent. The fractional loss of 0.9 consists primarily of a loss of about 0.5 due to a reflection at the diode surface, and of losses due to recombination at the surface and in the bulk of the n-type layer. No attempts have been made to reduce these factors in the present devices.

The speed of the photovoltaic response was measured by means of light pulses from a GaAs diode laser, which had a risetime of less than 1 nsec. The time constant of the photovoltage pulse observed by connecting a properly terminated 50-ohm line directly to the detector diode was about 200 nsec at 12°K and about 20 nsec at 77°K. The 200 nsec value provides an estimate of the carrier lifetime at 12°K. The 20 nsec value is an upper limit to the 77°K lifetime, since at 20 nsec the capacitance of the diode could be a limiting factor to the response. The lower lifetime at 77°K may partly account for the reduced responsivity at this temperature, as shown in Fig. I-2, because the fraction of generated carriers which reach the junction is directly related to the diffusion length.

The rms noise voltage at 12°K was found to be approximately proportional to the reciprocal of the frequency between 500 and 3000 Hz. At the 900 Hz chopping frequency, where the above responsivity measurements were made, a noise voltage of 3×10^{-10} V sec$^{1/2}$ was determined at 12°K. This corresponds to a noise equivalent power of about 5×10^{-12} W sec$^{1/2}$ and a D* of 8×10^{9} cm/W sec$^{1/2}$ at the 11 μ wavelength.

Figure I-3 shows the spectral dependence of the open-circuit responsivity of a $Pb_{0.83}Sn_{0.17}Te$ diode at zero bias. The responsivity and D* for this diode are about the same or slightly larger than for the previous diode. The responsivity cutoff, taken at 50 percent of the peak responsivity is 14 μ at 12°K and 11 μ at 77°K. This means that at 12°K this diode responds throughout the atmospheric window and at 77°K it will detect the CO_2 laser radiation at 10.6 μ. The time response of the $Pb_{0.83}Sn_{0.17}Te$ detector at 77°K to a Q-switched CO_2 laser pulse is shown in Fig. I-4. Figure I-5 shows the variation of the energy gap with alloy composition at both 12°K and 77°K as determined by luminescence data[1,2,3] and by the photovoltage measurements. The temperature coefficient of the energy gap of the alloys between 12°K and 77°K agrees closely with the temperature coefficient in PbTe, and the energy gap at 77°K decreases with increased Sn concentration with a slope nearly equal to the slope at 12°K. These observations lend further support to the model for the band structure of the alloys.[1]

I. Melngailis   T. C. Harman
A. R. Calawa   J. O. Dimmock
J. F. Butler

B. DIODE LASERS OF $Pb_{1-y}Sn_ySe$ AND $Pb_{1-x}Sn_xTe$

We should like to report the observation of infrared laser emission at 12°K and 77°K from diodes of $Pb_{1-y}Sn_ySe$ and $Pb_{1-x}Sn_xTe$. Optically pumped infrared laser emission in $Pb_{1-x}Sn_xTe$ at 12°K has recently been observed.[1] From those and other experiments,[4,5] it was concluded[1] that the energy gap of $Pb_{1-x}Sn_xTe$ at 12°K decreases smoothly with increasing Sn concentration, becoming zero at x = 0.35. Our current results show that the energy gap of $Pb_{1-y}Sn_ySe$ also decreases with a decreasing Pb:Sn ratio,[†] and indicate that the value of y for zero energy gap at 12°K lies within the range $0.11 \leqslant y \leqslant 0.14$. This work demonstrates that diode laser action over a wide range in the infrared can be attained with the (Pb, Sn) salts.

$Pb_{1-y}Sn_ySe$ crystals were vapor-grown at 825°C, using a 10-gm powdered source ingot of composition y = 0.05, and air-cooled from the growth temperature. The source ingot was prepared from a 100-gm stoichiometric mixture of the components that had been heated above the melting point and water-quenched. Vapor-grown crystals and the quenched ingot were n-type. A diffused p-type skin was produced by heating the crystals for one hour at 400°C with a vapor source of Se-saturated PbSe. Crystal growth, ingot preparation and diffusion runs were carried out in evacuated, sealed quartz ampules. Electron beam microprobe analysis yielded a value of y = 0.032 on the diffused surface and y = 0.044 in the crystal bulk. In the p-n junction region, y is expected to have an intermediate value. Diodes in the form of rectangular parallelepipeds were made by cleaving along {100} surfaces, and were mounted in low inductance packages, using a low melting temperature Hg-In-Tl solder.

$Pb_{1-x}Sn_xTe$ crystals for several values of x were vapor grown by a similar method. Growth temperatures were between 700°C and 825°C. For nominal values of x between 0.16 and 0.20 p-type vapor grown crystals were obtained using metal saturated source powders. An n-type skin formed during the cooling process. For $x \leqslant 0.10$, n-type $Pb_{1-x}Sn_xTe$ was vapor grown from metal saturated source powders and a p-skin was formed subsequently by diffusion using a Te-saturated PbTe source. Diode lasers have also been fabricated from Bridgman-grown $Pb_{1-x}Sn_xTe$. The $Pb_{1-x}Sn_xTe$ diodes were shaped and packaged in the same manner as were the $Pb_{1-y}Sn_ySe$ devices.

For spectral measurements, diodes were mounted on the cold finger of a liquid helium dewar equipped with KRS-5 windows. The diodes were pulse excited, although CW operation at 12°K was possible in both $Pb_{1-y}Sn_ySe$ and $Pb_{1-x}Sn_xTe$ devices. Spectra were measured using a NaCl prism monochromator, a copper-activated germanium detector and a lock-in amplifier system.

Figure I-6 shows the 12°K spectra for a $Pb_{1-y}Sn_ySe$ diode at current levels below and above the threshold for stimulated emission. Threshold current density at this temperature was $670 \, A \, cm^{-2}$. The Fabry-Perot cavity length was $315 \, \mu$. Using this value the observed mode spacing gives a value of 6.4 for the quantity $(n_o - \lambda_o \, dn/d\lambda)$. At a temperature of 77°K, the threshold current density was $2700 \, A \, cm^{-2}$ and laser action occurred at $10.2 \, \mu$. The emission data of Fig. I-6 indicate an energy gap at 12°K of 0.100 eV in the p-n junction region of the $Pb_{1-y}Sn_ySe$ device, while the energy gap of pure PbSe at this temperature is 0.145 eV.[6] This

---

[†] A. J. Strauss has previously obtained this result from optical absorption measurements on thin films of $Pb_{1-y}Sn_ySe$ for $0 \leqslant y \leqslant 0.20$.

3-85-5390(1)

WAVELENGTH (μ)

750 A cm^{-2}

650 A cm^{-2}

RELATIVE INTENSITY

PHOTON ENERGY (eV)
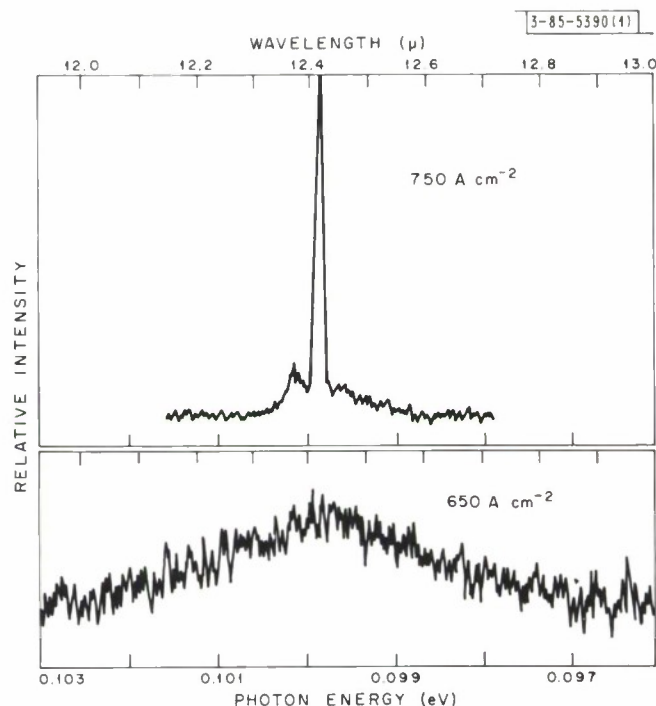
Fig. I-6. Emission spectra for $Pb_{1-y}Sn_ySe$ diode laser at approximately 12°K.

dependence of energy gap on Sn concentration for $Pb_{1-y}Sn_ySe$ is similar to that for $Pb_{1-x}Sn_xTe$. Linear extrapolations using the energy gap of 0.145 eV at y = 0 and 0.100 eV at the various y-values found by electron beam microprobe measurements on the laser diode indicate a zero energy gap at 12°K in $Pb_{1-y}Sn_ySe$ for some value of y between 0.11 and 0.14.

Spontaneous and coherent emission spectra for a $Pb_{0.83}Sn_{0.17}Te$ diode at 12°K are given in Fig. I-7. The threshold current density is 600 A cm^{-2}. The cavity end faces were 220 μ apart. Using this value the mode spacing gives a value of 6.9 for $(n_o - \lambda_o dn/d\lambda)$. At 77°K laser action at 10.6 μ was observed with a threshold current density of 3,000 A cm^{-2}. Diode laser action at 12°K for other values of x in the $Pb_{1-x}Sn_xTe$ system was observed at 13.7, 12.7 and 9.4 μ. The dependence of emission wavelength on Sn concentration in the $Pb_{1-x}Sn_xTe$ diodes is in substantial agreement with Fig. 3 of Ref. 1.

J. F. Butler
A. R. Calawa
T. C. Harman

C. THE GaAs-InSb GRADED-GAP HETEROJUNCTION

A paper entitled "The GaAs-InSb Graded-Gap Heterojunction" has been submitted to Solid-State Electronics. The abstract of the paper follows:

The interface-alloy technique has been used to produce heterojunctions between GaAs and InSb. X-ray and Kossel line patterns show that, despite the relatively large 14% lattice mismatch between the semiconductors, these heterojunctions are
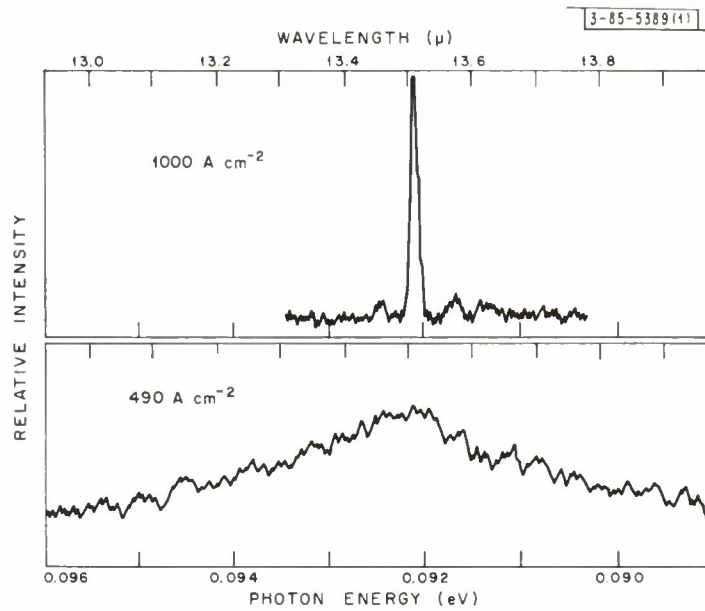
Fig. I-7. Emission spectra for $Pb_{0.83}Sn_{0.17}Te$ diode laser at approximately 12°K.

single-crystal. Electron beam microprobe analysis indicates that the inter-diffusion of the four elements is smaller than the 1.9 µ diameter of the beam. Photocurrent and current-voltage measurements are explained by a model for the heterojunction band structure in which the salient feature is a region of the order of 60 Å long which has a linearly-graded energy gap joining the GaAs to the InSb. In addition, interface states "fix" the location of the GaAs bands at the heterojunction interface such that, at room temperature, the conduction band extrapolates to a value approximately 0.93 eV above the Fermi level. The heterojunction barrier maximum is smaller, however, because a portion of the GaAs depletion layer potential is developed across the graded-gap region. The photocurrent occurs via hot carriers generated in the graded-gap region which traverse this region (with a mean free path of approximately 20 Å) to the heterojunction barrier maximum. As predicted by the model, incident monochromatic radiation of energy smaller than the GaAs bandgap produces a photocurrent which varies exponentially with photon energy as $I_0 \exp[C(h\nu - E_g)]$, where C is a positive parameter which decreases for increasing reverse bias on the heterojunction, and I_0 is the extrapolated response at the GaAs bandgap, which is independent of applied bias. The forward current of units fabricated with n-type GaAs varies as $\exp(qV/\eta kT)$, and, except at lower temperatures where tunneling becomes important, the values of η as a function of the GaAs impurity doping concentration can be explained in terms of the increase in the heterojunction barrier height with voltage, as predicted by the graded-gap model. Similarly, the voltage dependence of the reverse current is quantitatively explained by this model. The results of the capacitance-voltage measurements

are consistent with the current-voltage and photocurrent measurements evaluated in terms of the graded-gap heterojunction model.

E. D. Hinkley
R. H. Rediker†

D. ION IMPLANTATION OF PHOSPHORUS IN GERMANIUM

A 400 keV Van de Graaf positive ion accelerator has been used to implant phosphorus ions in germanium. Experimental evidence indicates that the implanted ions have produced n-type regions in bulk p-type material. Phosphine (PH_3) gas located at the positive terminal of the accelerator passes through a controlled "leak" into a high-frequency discharge tube where the gas is ionized. The ionized components are accelerated along an evacuated column into the field of an electromagnet which analyzes the beam and deflects the phosphorus ions onto the germanium target. A polished [111] germanium surface, inclined slightly from normal incidence in order to reduce the probability of channeling, was exposed to the impinging phosphorus beam. The 340 keV phosphorus beam was circular in cross-section with a diameter of 2 mm. Implantation proceeded for one hour with an incident phosphorus beam current of 0.4 μA, yielding a total of 9×10^{15} implanted atoms. Assuming that the phosphorus atoms are distributed uniformly over a distance of approximately 2 μ along the direction of incidence, the concentration of phosphorus atoms in the implanted region is of the order of 1×10^{21} cm^{-3}.

No observable macroscopic surface damage was produced by the implantation, although the exposed region did become darker. Examination with an electron beam microprobe indicated that the phosphorus concentration at the sample surface was of the order of 1×10^{20} cm^{-3}. The implanted germanium wafer was angle-lapped and stained with a $CuSO_4$-HF solution. Microscopic examination indicated that the n-type region was approximately 2 μ deep.

Whereas the unimplanted germanium showed p-type surface conductivity, thermal probe measurements indicated that the implanted region was definitely n-type. Post-implantation annealing was not required, although in cases where it was performed the n-type conductivity was enhanced. A 250-μ diameter tin sphere was alloyed on the implanted side of the germanium in the unexposed p-type region in order to establish a "reference" p-n junction, and a 25-μ diameter tin sphere was alloyed on the implanted n-type region to serve as an ohmic contact. (The small size of this latter sphere reduced the possibility of alloying through the narrow implanted region.) The unimplanted side of the germanium specimen was alloyed to an indium-clad molybdenum tab for ohmic contact. Both p-n junctions exhibited diode behavior, but the forward current corresponding to a particular bias voltage was substantially larger for the ion-implanted junction than for the "reference" junction. This confirms that the 2-mm diameter implanted region is responsible for the observed germanium p-n junction characteristics.

E. D. Hinkley

E. BULK GaAs NEGATIVE CONDUCTANCE AMPLIFIERS

Negative conductance microwave amplifiers of high-resistivity n-GaAs were first reported by Thim et al.[7] and have been studied considerably since.[8-11] Although it has been assumed

---

† Department of Electrical Engineering and Center for Materials Science and Engineering, M.I.T.

from the outset that the effect was due to a bulk differential negative resistance arising from the transferred-electron mechanism[12] (which results in Gunn oscillations[13] in lower resistivity material), this interpretation has never been clearly established. Computer calculations by McCumber and Chynoweth[11] based on their two-valley transferred-electron model yielded a negative conductance at the right frequency, but did not give correct values of the gain or oscillation threshold. Similar inconclusive results were obtained[14] analytically using a three-slope piecewise-linear approximation to the drift velocity-electric field relation. However, both calculations assumed a rather small value for the negative mobility, whereas recent theories of the electron transfer[15,16] and of the domain dynamics[17,18] suggest a much larger negative mobility.[†]

By taking the negative mobility as an adjustable parameter, we have now obtained good quantitative agreement between the measured small-signal admittance parameters of GaAs negative conductance amplifiers and those calculated from the three-slope piecewise-linear model for v vs E. The calculation yields a negative mobility of about 2500 to 3000 cm^2/V sec, which is quite consistent with the transferred-electron model. Because of the sensitivity of the fit to the value of the negative mobility, the above result should be fairly accurate and perhaps constitutes the best present estimate of the negative mobility.[‡]

The devices were prepared by alloying ohmic tin contacts to opposite faces of chips of 4-ohm-cm n-GaAs, and mounting the resulting sample in a small varactor diode package. Each device was then placed at the end of a 50-ohm coaxial slotted line, cooled to reduce its carrier concentration into the proper range for amplification (about $10^{13} cm^{-3}$ for a sample length of $50\,\mu$) and biased on a pulse basis to avoid heating. The admittance of the samples was measured with the slotted line over a range of frequencies centered around the frequency of maximum reflection gain. Figure 1-8 shows the data for one of the devices. The sample, which was prepared from n-GaAs of 4-ohm-cm room temperature resistivity, was $50\,\mu$ long and $1.75 \times 10^{-3} cm^2$ in area. At the operating temperature of $-40°C$ the carrier concentration was $1.6 \times 10^{13} cm^{-3}$ and the low-field mobility was $6000\ cm^2/V$ sec; the bias was 29 V. The values of the adjustable parameters used above were $\mu_2 = -2500\ cm^2/V$ sec, $\mu_3 = 0$, and $v_v = 0.4\,v_p$. The case capacitance of 0.5 pF ($300\ pF/cm^2$) was added to the calculated capacitance to give the solid line shown in the lower part of the figure. Essentially identical results were obtained for the other samples from the same crystal.

In the upper part of Fig. 1-8, the conductance per unit of sample area is shown by the open data points for the frequency range of 2.5 to 5 GHz. In the lower part, the susceptance is plotted as an effective capacitance per unit of sample area by dividing the measured susceptance by the radian frequency and the sample area. Calculated conductance and capacitance curves which will be discussed later are also shown. As may be seen, there is a broad region of negative conductance, followed by a sharp rise to positive conductance. The capacitance, on the other hand, remains positive over this frequency range, with a peak near the zero crossing of the conductance.

[†] Mahrous and Robson[19] have calculated the impedance of GaAs amplifiers using a three-slope approximation to the v vs E curve of Butcher and Fawcett,[15] but they did not attempt a comparison with experiment.

[‡] Gunn and Elliott[20] have recently inferred from very short pulse measurements on GaAs that the negative mobility is only about $300\ cm^2/V$ sec. However, Copeland, in a private communication, has shown that their observations can be explained with a negative mobility of the size found here if the low-field hole generation rate which he deduced from other experiments[21] is taken into account. The extent to which such hole generation would modify the present results has not yet been determined.
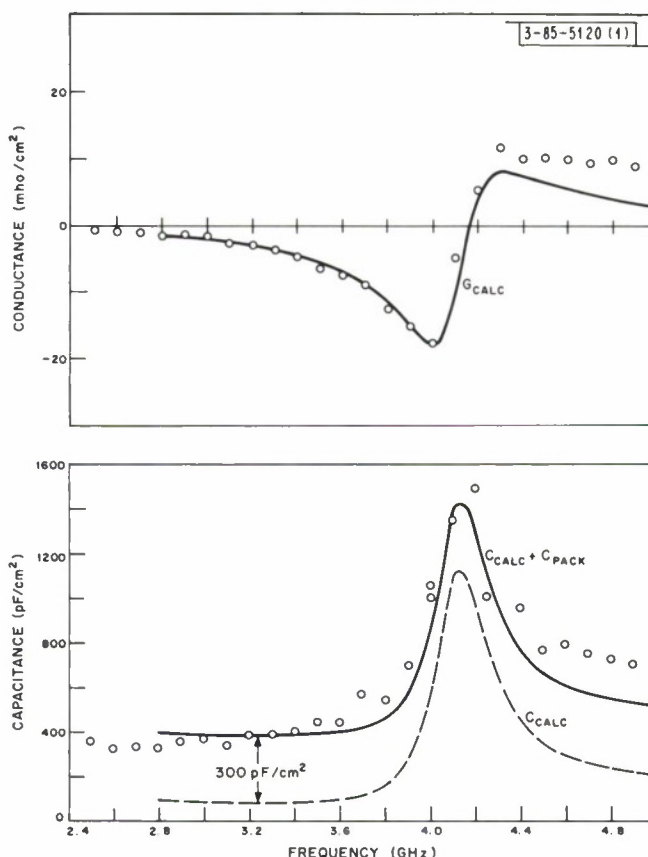
Fig. I-8. Comparison of measured small-signal conductance and capacitance per unit area (open circles) with calculations (solid lines) based on v vs E curve of Fig. I-9.

As a partial check on the accuracy of the measurements, the data of Fig. I-8 were used to compute the reflection gain expected from the device in a 50-ohm reflection amplifier. The computed gain agreed with the measured values within ±0.5 dB over the frequency range of 2.5 to 5 GHz.

We have attempted to fit the data, using the three-slope piecewise-linear approximation, to the v vs E curve shown in Fig. I-9. The values of peak drift velocity v_p and peak electric field E_p were taken as 2×10^7 cm/sec and 4000 V/cm, respectively, based on threshold measurements for Gunn effect oscillators at T = −40°C. The value of μ_1, which represents some average positive mobility, was thus taken as 5000 cm^2/V sec, slightly less than the experimental low-field value of 6000 cm^2/V sec. The mobilities μ_2 and μ_3 and the valley drift velocity v_v were considered as adjustable parameters, although the results are sensitive only to μ_2.

The spatially nonuniform[22] steady-state solution may be obtained to a good approximation by neglecting diffusion and assuming a virtual-cathode (E = 0) boundary condition at the negative contact. For the AC solution we assume a small-signal perturbation varying sinusoidally in time, assume that the drift velocity at each point instantaneously follows the local electric
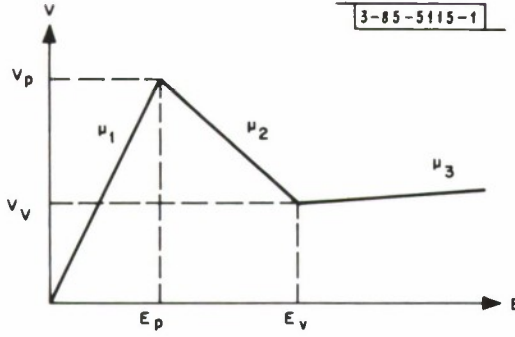
Fig. I-9. Piecewise-linear approximation of drift velocity–electric field relation of n-GaAs used in admittance calculation.

field,[†] and again neglect diffusion. Under these assumptions and approximations, Poisson's equation and the continuity equation combine to yield[11] a linear first-order differential equation for the small-signal electric field E_1:

$$\epsilon v(x)\,(\partial E_1/\partial x) + [i\omega\epsilon + n(x)\,e\mu(x)]\,E_1 = J(\omega) \tag{1}$$

where $v(x) = v[E(x)]$ is the steady-state electron velocity, $n(x)$ the steady-state electron density, $\mu = dv/dE$ the mobility, ϵ the GaAs permittivity, and $J(\omega)$ the total current density (including displacement current) at frequency ω. Solving Eq. (1) with $E_1 = 0$ at the virtual cathode at $x = 0$ and integrating the electric field to obtain the small-signal voltage $V(\omega)$, we obtain for the impedance of a sample of length L

$$Z(\omega) = \frac{V(\omega)}{J(\omega)} = \int_0^L dx_1 \int_0^{x_1} dx_2\, \frac{e^{i\omega[\tau(x_2)-\tau(x_1)]}}{\epsilon v(x_2)}\, \frac{n(x_1) - n_o}{n(x_2) - n_o} \tag{2}$$

where n_o is the equilibrium electron density and

$$\tau(x) = v^{-1}(x)\,[x + \epsilon E/en(x)] \tag{3}$$

is the signal transit time.

The assumption of a piecewise-linear v vs E relation allows Eq. (2) to be integrated easily, although the resulting expression is rather involved.[‡] However, it is a simple matter to evaluate the impedance numerically for a wide range of parameters. The calculated curves in Fig. 1-8 are for $\mu_2 = -2500\ \text{cm}^2/\text{V sec}$, $\mu_3 = 0$ and $v_v = 0.4\,v_p$. The bias voltage V_o and the equilibrium carrier concentration were set equal to their experimental values, which were $V_o = 29\ \text{V}$ and $n_o = 1.6 \times 10^{13}\ \text{cm}^{-3}$. Good agreement is found for the conductance over the frequency range 2.5 to 4.2 GHz. Above 4.2 GHz, the data may be somewhat inaccurate because the admittance measurements involved Smith chart rotations of nearly one-half of a wavelength from the reference short circuit. For the capacitance, the case capacity of about 0.5 pF (300 pF/ cm^2) must be added to the calculated curve; quite satisfactory agreement is obtained when this correction is made.

---

† The intervalley transfer rate estimated in Ref. 16 is much greater than our maximum frequency of 5 GHz.

‡ If $\mu_3 = 0$, the expression simplifies considerably; the result for this case is given in Ref. 20.

The ranges over which the adjustable parameters could be varied with substantially the same agreement were $-3000 < \mu_2 < -2500 \, cm^2/V \, sec$, $-250 < \mu_3 < 250 \, cm^2/V \, sec$, and $0.2 < v_v/v_p < 0.5$. Note that μ_3 was allowed to take on negative values in order to simulate more complex negative mobility characteristics. As indicated by the above ranges, the calculated admittance is sensitive only to the (initial) mobility μ_2, which therefore permits a rather good determination of μ_2.

The same set of parameter values that explain the admittance data also provide both a reasonable fit to the measured current-voltage characteristics and a prediction of the correct frequency and threshold bias for oscillation.

Besides these results in the 3- to 4-GHz range, we have some preliminary admittance data for devices operating in the 10-GHz range which can apparently be fit with the same velocity-electric field relation. Also, this model is able to explain the very rapid variation of gain with temperature reported by Thim.[23]

In conclusion, the piecewise-linear model can account for the behavior of n-GaAs negative conductance amplifiers and in addition provides a good estimate of the (initial) negative mobility for GaAs.

A. L. McWhorter
A. G. Foyt

F. EPITAXIAL GaAs GUNN EFFECT OSCILLATORS

Although Gunn effect oscillators made from epitaxial GaAs have been reported by several workers,[24-27] none of these devices operated with power conversion efficiencies as great as those obtained for devices made on bulk material.[28,29] We wish to report a substantial improvement in the efficiency of such oscillators made with epitaxial material. Efficiencies as high as 9 percent have been obtained for a device delivering a peak output power of 1.75 watts at 9.3 GHz.

The epitaxial films were deposited on GaAs substrates using the process described previously.[30] This process, first discussed by F. R. Knight et al.[31] and more recently by other workers,[32,33] operates as follows: $AsCl_3$ and H_2 enter the hot zone of the furnace and react to form As and HCl. The HCl and Ga react to form GaCl, and the As and GaCl are transported down the reaction tube to the substrate. At the (lower) substrate temperature, the GaCl reacts with the As to form GaAs and $GaCl_3$. The GaAs deposits on the substrate as an epitaxial film.

We have had to take two precautions in addition to those already mentioned in the literature, in order to obtain reproducible films suitable for Gunn effect oscillators. First, a temperature gradient must be maintained in the substrate zone in order to obtain a reproducible thickness of the epitaxial layer.† Second, a prolonged soak of the substrates in hot potassium cyanide is necessary to prevent the occurrence of a p-type layer between the substrate and the epitaxial film. This treatment presumably removes copper from the surface of the substrate.

Some of our best results using this process are shown in Table I-1. All these evaluations were made on layers deposited on chromium-doped semi-insulating substrates. As may be seen, the best layers have electron concentrations in the high 10^{14} to low $10^{15} \, cm^{-3}$ range, both at room temperature and at 77°K. The electron mobilities for these layers are typically

---

† For a gradient of 10°C per inch, typical deposition rates are about 100 μ per hour for a {111} A face, and about 20 μ per hour for a {100} face.

TABLE I-1 BEST EPITAXIAL GROWTH RESULTS				
Sample	n (300°K) (cm^{-3})	n (77°K) (cm^{-3})	μ (300°K) (cm^2/V sec)	μ (77°K) (cm^2/V sec)
042-2-2	1.2×10^{15}	1.2×10^{15}	8,000	54,000
043-4	6.0×10^{14}	6.1×10^{14}	8,400	73,000
043-1-2	5.7×10^{14}	5.8×10^{14}	8,200	77,000

TABLE I-2 SUMMARY OF OSCILLATOR RESULTS					
Epitaxial Layer Thickness (μ)	(nl) (cm^{-2})	Bias Voltage (V)	Output Frequency (GHz)	Peak Output Power (W)	Efficiency (percent)
30	6×10^{12}	42	2.5	3.2	7.5
20	4×10^{12}	11	5.0	1.6	6.5
10	2×10^{13}	15	8.35	2.5	9
10	2×10^{13}	18	9.3	1.75	9

$8000\,cm^2/V$ sec at room temperature, and increase at $77°K$ to values as high as $77,000\,cm^2/V$ sec.

We have made Gunn effect oscillators from similar films deposited on heavily doped sub-strates. The devices were fabricated by pla ing the wafer on a tin clad molybdenum tab and by alloying the tin to the GaAs in a reducing atmosphere. A tin dot is then alloyed onto the epitaxial layer at temperatures between 400 and 500°C in the same reducing atmosphere. The excess GaAs outside the area of the tin dot is etched away, and the resulting sample is mounted in a standard varactor diode package for further testing. The device is then placed in a tunable coaxial cavity and biased on a pulse basis. The RF output power is measured with a thermistor power meter and the output frequency monitored with a spectrum analyzer through a directional coupler. At each bias setting, the cavity was adjusted for peak output power. Some of the best results obtained to date are summarized in Table I-2.

The epitaxial layer thickness for these devices ranged from 30 to $10\,\mu$ and the output frequencies ranged from 2.5 to 9.3 GHz. Some of these devices could be biased to average electric fields over 10,000 V/cm, and gave up to 9 percent efficiency. We also note that the carrier concentration — sample length products (nl) for these samples are considerably larger than the value of about $2 \times 10^{12}/cm^2$ which has been proposed as an optimum for oscillator efficiency.

In conclusion we feel that this work has shown that Gunn oscillators with relatively high efficiencies can be fabricated using epitaxially grown GaAs and that both the preparation of the epitaxial material and the method of contacting, as well as careful design of the resonant cavity, are important in the high efficiency which these devices have shown.

A.G. Foyt
C.M. Wolfe

REFERENCES

1. J. O. Dimmock, I. Melngailis and A. J. Strauss, Phys. Rev. Letters **16**, 1193 (1966).

2. J. F. Butler, A. R. Calawa, R. J. Phelan, Jr., T. C. Harman, A. J. Strauss and R. H. Rediker, Appl. Phys. Letters **5**, 75 (1964).

3. K. F. Cuff, Proceedings of the Symposium on Radiative Recombination in Semiconductors (Dunod, Paris, 1965), pp. 11-20.

4. P. M. Nikolic, Brit. J. Appl. Phys. **16**, 1075 (1965).

5. E. G. Bylander, private communication.

6. J. F. Butler and A. R. Calawa, Physics of Quantum Electronics (McGraw-Hill, New York, 1966), p. 458.

7. H. W. Thim, M. R. Barber, B. W. Hakki, S. Knight and M. Uenohara, Appl. Phys. Letters **7**, 167 (1965).

8. H. W. Thim and M. R. Barber, IEEE Trans. Elect. Dev. **ED-13**, 114 (1966).

9. B. W. Hakki and S. Knight, IEEE Trans. Elect. Dev. **ED-13**, 94 (1966).

10. A. G. Foyt and T. M. Quist, IEEE Trans. Elect. Dev. **ED-13**, 199 (1966).

11. D. W. McCumber and A. G. Chynoweth, IEEE Trans. Elect. Dev. **ED-13**, 4 (1966).

12. B. K. Ridley and T. B. Watkins, Proc. Phys. Soc. **78**, 293 (1961); C. Hilsum, Proc. IRE **50**, 185 (1962).

13. J. B. Gunn, IBM J. Res. Develop. **8**, 141 (1964).

14. A. L. McWhorter, International Electron Devices Meeting, Washington, D. C., October 20-22, 1965.

15. P. N. Butcher and W. Fawcett, Proc. Phys. Soc. **86**, 1205 (1965); Physics Letters **21**, 489 (1966).

16. E. M. Conwell and M. O. Vassell, IEEE Trans. Elect. Dev. **ED-13**, 22 (1966).

17. P. N. Butcher, Phys. Letters **19**, 546 (1965); P. N. Butcher, W. Fawcett and C. Hilsum, Brit. J. Appl. Phys. **17**, 841 (1966).

18. J. A. Copeland, IEEE Trans. Elect. Dev. **ED-13**, 189 (1966); J. Appl. Phys. **37**, 3602 (1966).

19. S. Mahrous and P. N. Robson, Electronics Letters **2**, 107 (1966).

20. J. B. Gunn and B. J. Elliott, Physics Letters **22**, 369 (1966).

21. J. A. Copeland, Appl. Phys. Letters **9**, 140 (1966).

22. W. Shockley, Bell Syst. Tech. J. **33**, 799 (1954).

23. H. W. Thim, IEEE Trans. Elect. Dev. (to be published).

24. C. Hilsum, K. C. H. Smith and B. C. Taylor, Electronics Letters **6**, 178 (1965).

25. T. C. Hasty, P. A. Cunningham and W. R. Wisseman, IEEE Trans. Elect. Dev. **ED-13**, 114 (1966).

26. D. Brady, S. Knight, K. Lawley and M. Uenohara, as quoted by B. C. DeLoach, Microwave Journal **9**, 97 (1966).

27. L. E. Norton and D. L. Thomson, as quoted by B. C. DeLoach, Microwave Journal **9**, 97 (1966).

28. T. M. Quist and A. G. Foyt, Proc. IEEE **53**, 303 (1965).

29. D. G. Dow, C. H. Mosher and A. B. Vane, IEEE International Electron Devices Meeting, Washington, D. C., October 20, 1965.

30. C. M. Wolfe, T. M. Quist and A. J. Strauss, Solid State Research Report, Lincoln Laboratory, M.I.T. (1966:2), p. 7, DDC 639064.

31. F. R. Knight, D. Effer and P. R. Evans, Solid State Electronics **8**, 178 (1965).

32. D. Effer, J. Electrochem. Soc. **112**, 1020 (1965).

33. J. Whitaker and D. E. Bolger, Solid State Communications **4**, 181 (1966).

II. OPTICAL TECHNIQUES AND DEVICES

A. OPTIMUM HETERODYNE DETECTION AT $10.6\,\mu$m IN PHOTOCONDUCTIVE Ge:Cu

Using a Ge:Cu photoconductor as a heterodyne detector[1-3] at $10.6\,\mu$m, we have observed a minimum detectable power which is within a factor of 10 of the theoretical quantum limit, $h\nu B$. In the experimental arrangement used, the radiation from a CO_2-N_2-He laser, emitting approximately 10 watts at $10.6\,\mu$m, was incident on a modified Michelson interferometer (see Fig. II-1). One mirror of the conventional interferometer was replaced by an off-center rotating aluminum wheel with a roughened surface. The diffusely scattered radiation from the wheel provided a Doppler shifted signal which was recombined at the beam splitter with the unshifted (or local oscillator) radiation reflected from the mirror of the other interferometer leg.
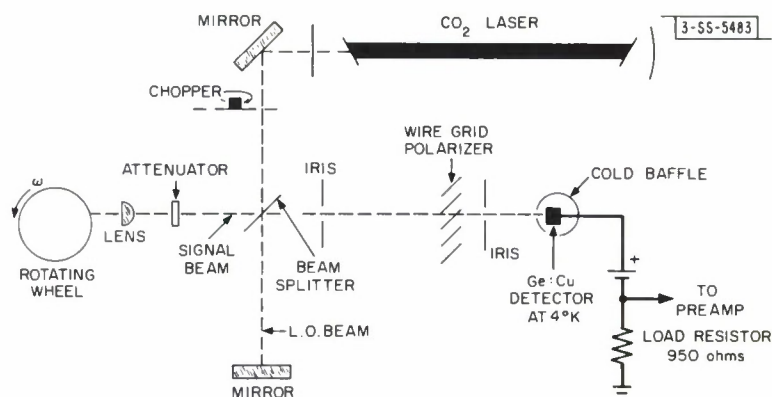
Fig. II-1. Experimental arrangement of heterodyne detection system.
Electric field vector lies perpendicular to plane of paper.

Figure II-1 shows the experimental setup. A 2.54-cm focal length Irtran II lens inserted in the signal beam focused the radiation to a single point on the rim of the rotating wheel. The function of the lens was to collect sufficient scattered radiation to permit an incoherent (non-heterodyne) measurement of the scattered signal power at the detector for calibration purposes, and to insure spatial coherence of the scattered radiation at the detector.[4] Irises were used to maintain the angular alignment of the wave fronts of the two beams to $\sim$2 mrad, which is well within the required angular tolerance for optimum photomixing ($\lambda/a \sim 5$ mrad for a detector aperture $a = 2$ mm).[2] A Perkin-Elmer wire-grid polarizer insured that the recombined beams had a common linear polarization.

With a bias voltage of 13.5 volts on the Ge:Cu detector, its (incoherent) low-power responsivity was found to be 0.2 amp/watt by calibration with a black-body source of known temperature. The heterodyne signal obtained from the load resistor was fed into a thermocouple-type rms voltmeter through a controlled-bandwidth low-noise preamplifier. Alternately, the load resistor output was fed simultaneously to an oscilloscope and to a spectrum analyzer.

The results of a typical measurement are shown in Fig. II-2. The solid line is the observed signal-to-noise power ratio $(S/N)_{power}$ of the heterodyne signal as a function of the signal beam

3-SS-5484
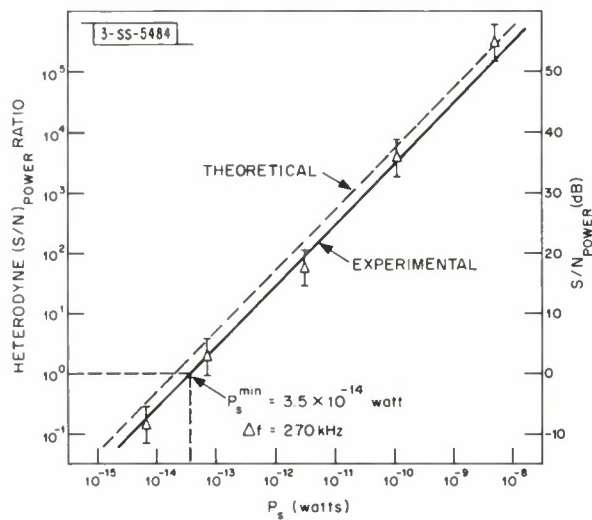
Fig. II-2. Theoretical and experimental values of signal-to-noise power ratio as a function of signal power.

Fig. II-3. (a) Multiple-sweep display of heterodyne signal. Loss of definition of waveform in third cycle reflects finite bandwidth of heterodyne signal. (b) Single sweep of heterodyne signal shown in (a), but with a longer time scale. Modulation of signal envelope arises from random nature of scattering surface.

-82-5365-1

16
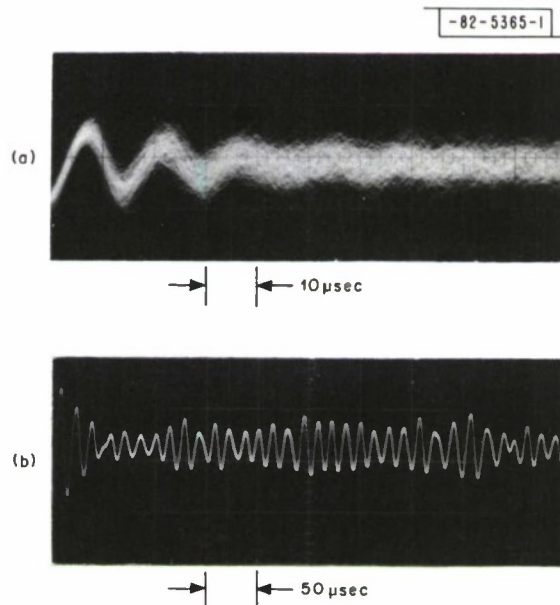
radiation power (P_s) for a typical run. Only noise arising from the presence of the L.O. beam (which was the dominant contribution to the noise) is considered. Various values of P_s were obtained by inserting calibrated CaF_2 attenuators in the signal beam, while the unattenuated power was measured by chopping the signal beam in the absence of the L.O. With a heterodyne signal centered at about 70 kHz, and an amplifier bandwidth of 270 kHz, the experimentally observed minimum detectable power P_s^{min} (defined as that signal beam power for which the heterodyne S/N is unity) is seen to be 3.5×10^{-14} watts. This corresponds, in a 1 Hz bandwidth, to a minimum detectable power of 1.3×10^{-19} watt. Measurements were made with an L.O. power of 1.5 mw. A plot of the theoretical expression[1,3] $(S/N)_{power} = \eta P_s / 2h\nu\Delta f$, which includes the effect of g-r (generation-recombination) noise from the photoconductor[5,6] is also shown in Fig. 11-2. With an assumed quantum efficiency $\eta = 1/2$, it is seen to lie above the experimental curve by a factor of approximately 2, but within the limit of experimental accuracy. Had noise from sources other than the L.O. been taken into account in computing the S/N, the experimental curve would be a factor of 3 below the theoretical. Although the signal-to-noise ratio agrees closely with theory, the observed values of signal and noise[5,6] are higher than calculated on the basis of the measured responsivity. An explanation for this observation is being sought in a possible dependence of the photoconductor gain on the frequency or on the power of the incident radiation.

Figure 11-3(a) shows a multiple sweep display of the heterodyne signal obtained with a signal power of 1.0×10^{-8} watt. The loss of definition of the waveform in the third cycle reflects the finite bandwidth of the heterodyne signal. Figure Il-3(b) shows a single trace of this signal for a longer time scale. The modulation bandwidth is caused by statistical fluctuations of the heterodyne signal arising from the moving diffuse surface of the wheel. For the experimental configuration used, where the roughness of the wheel ($\sim 10\,\mu$m) is comparable to the size of the focused spot on the wheel ($\sim 50\,\mu$m), the bandwidth of the noise modulation, B, should be approximately[4] v/d. Here, v is the velocity at which the illuminated spot traverses the surface, and d is the diameter of the focused spot on the wheel. With $v = r\omega$ and $d \sim f\lambda/D$, B is given approximately by $r\omega D/F\lambda$. Here v is the tangential velocity of the wheel (157 cm/sec), ω is its angular velocity ($10\pi\,sec^{-1}$), and r its radius (5.05 cm). F represents the focal length of the lens (2.54 cm), while D is the diameter of the radiation beam at the output of the laser (~ 5 mm). Evaluating this, we obtain a calculated value B ~ 30 kHz which is comparable to values observed on the spectrum analyzer.

M. C. Teich
R. J. Keyes
R. H. Kingston

B. CARBON DIOXIDE 10.6 MICRON LASER

A sealed off Brewster window laser of a design similar to the one mentioned in Solid State Research Report (1966:2) was operated to determine the useful life of the gas mixture as a function of the power output at $10.6\,\mu$. This water jacketed tube of 10 mm bore and 70 cm discharge length between kovar electrodes, was used in a one meter half confocal cavity with output coupling through multiple layer coated Irtran II mirror which had a 22 percent transmission. The tube and 1.3 liter reservoir were filled with a mixture of 2 torrs CO_2, 2 torrs N_2, and 7 torrs He.
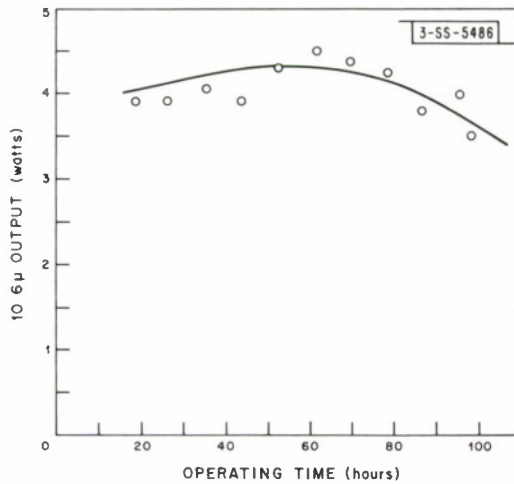
Fig. II-4. Output power of a sealed-off 10.6 μ CO_2 laser as a function of operating time.

This mixture was not accurately adjusted nor were the optical components chosen for maximum power efficiency. The maximum radiation to electrical power efficiency measured previously was 7 percent while this tube was operated at 3 percent.

Figure II-4 shows the output power as a function of operating time on the laser tube. The tube output power was essentially constant over 98 hours which were accumulated over one month with most of the data scatter shown due to tuning of the laser mirrors. This cavity configuration permitted tuning over several transverse modes, and the data indicated that a reasonable operating life can be expected from this type of molecular laser.

The visible spontaneous emission from the side of the tube was monitored throughout the operating time interval, and the determinations so far indicate that CO angstrom bands, N_2 second positive series bands, and CN cyanogen violet bands were present. The CO bands generally were much more intense during the beginning of the test, but degraded to the intensity level of the N_2 and CN bands after 50 hours of operation. Only a small decrease in intensity was observed for the N_2 and CN bands during the operation of the tube.

Unless there is a cyclic process, the formation of CN and CO will ultimately deplete the supply of CO_2 within the tube. An understanding of the chemical processes taking place during the discharge will permit a realistic appraisal of the expected operating life of this molecular laser, and may suggest possible means for extending its life and power efficiency.

R. J. Carbone

REFERENCES

1. A. E. Siegman, S. E. Harris, and B. J. McMurtry, "Optical Heterodyning and Optical Demodulation at Microwave Frequencies," Optical Masers, edited by J. Fox (Polytechnic Press, John Wiley and Sons, Inc., New York, 1963), p. 511.

2. A. E. Siegman, Appl. Opt. 5, 1588 (1966); also Proc. IEEE 54, 1350 (1966).

3. S. Jacobs and P. Rabinowitz, "Optical Heterodyning with a CW Gaseous Laser," Quantum Electronics III, edited by P. Grivet and N. Bloembergen, (Columbia University Press, New York, 1964), p. 481.

4. G. Gould, S. F. Jacobs, J. T. La Tourrette, M. Newstein, and P. Rabinowitz, Appl. Opt. 3, 648 (1964).

5. R. C. Jones, Proc. IRE 47, 1481 (1959).

6. A. van der Ziel, Fluctuation Phenomena in Semi-Conductors, (Academic Press, New York, 1959), pp. 22, 65.

III. MATERIALS RESEARCH

A. INTRODUCTION

The crystal structure of Nd_2O_2Te has been determined by computer analysis of x-ray powder diffraction data. The atomic arrangement is derived from the K_2NiF_4 structure, in which the rare earth atoms exhibit an unusual 9-fold coordination.

In order to determine the cause of the anomaly observed in the x-ray scattering of ZnSe, neutron diffraction measurements have been made on this compound at room temperature and liquid helium temperature. The results obtained so far are inconclusive because of difficulties in evaluating background intensity corrections.

The phase diagram of Ag_2Te at high pressure has been investigated by means of electrical resistivity and x-ray diffraction measurements. Evidence has been obtained for three high-pressure phases, two of which exist at room temperature.

Hysteresis of the first-order $B8_1 \rightleftarrows B31$ magnetic transition in MnAs has been studied by measuring the resistivity and magnetic susceptibility as functions of pressure and temperature. The experimental results, together with earlier data for $MnAs_{1-x}P_x$, show that the transition is due to a large exchange striction in the basal planes together with a volume-dependent Weiss molecular field and manganese atomic moment.

The retrograde solubility of Pb in PbS has been investigated by means of Hall coefficient measurements on n-type samples prepared by annealing and quenching single crystals containing excess Pb. The carrier concentration decreases with decreasing annealing temperature from 2.4×10^{19} cm^{-3} for 912°C to 1.3×10^{18} cm^{-3} for 350°C.

Measurements of the Hall coefficient vs temperature for S-doped GaSb have shown that the lowest donor level of S lies about 0.075 eV below the lowest conduction band at atmospheric pressure. The pressure dependence of resistivity at room temperature shows that this donor level is associated primarily with the conduction band minima at the (100) zone faces.

The magnetoresistance and Hall coefficient of high-purity and V-doped Ti_2O_3 single crystals have been measured at magnetic fields up to 218 kG. The high magnetoresistance of the high-purity samples at 4.2°K is inconsistent with a conventional one-band carrier transport mechanism. The p-type conductivity and negative magnetoresistance of V-doped Ti_2O_3 suggest that part of the V is present in the quadrivalent state.

Efficient pulsed laser operation has been obtained in Nd-doped YVO_4 single crystals. The threshold is only about 1 joule. This low threshold is due to the reduced Stark splitting of Nd^{+3} ions in YVO_4 and to substantial transfer of absorbed energy from the lattice to the Nd^{+3} ions.

A method employing PbTe and SnTe as standards has been developed for the determination of Pb and Sn in $Pb_{1-x}Sn_xTe$ alloys by electron microprobe analysis. The results are in good agreement with those obtained by wet chemical techniques.

B. CRYSTAL STRUCTURE OF Nd_2O_2Te FROM X-RAY POWDER DATA

Kent and Eick[1] have reported the preparation of a family of rare earth compounds with the general formula R_2O_2Te, where R is the rare earth element. In measurements on a compacted

TABLE III-1
OBSERVED VS CALCULATED X-RAY INTENSITIES FOR Nd_2O_2Te
($a = 4.023$ Å, $c = 12.78$ Å)

HKL	I_{obs}	I_{calc}	HKL	I_{obs}	I_{calc}
002	1.0	1.1	316, 307	17.0	17.0
101	0.9	0.9	323; 2, 0, 10		
103	100.0	100.0	0, 0, 12; 228	1.9	1.0
110	39.8	38.7	400; 1, 1, 12	4.7	4.4
112	1.8	0.9	318, 402		
105, 006, 114	19.4	19.4	309, 411; 2, 1, 11	3.5	3.5
211	0.6	0.3	1, 0, 13; 327		
116, 204	21.7	20.8	2, 2, 10; 413	12.2	12.2
107, 213	36.2	35.4	2, 0, 12; 330		
215, 206, 220	14.7	15.0	332		
109, 301	6.0	7.0	0, 0, 14; 415	8.0	7.4
217, 303; 0, 0, 10	13.8	14.4	406, 334		
310, 308, 312			3, 1, 10; 420		
305, 226	5.1	5.5	3, 0, 11; 329	11.7	12.5
314; 1, 1, 10			1, 1, 14; 336		
219, 321	8.3	8.0	2, 1, 13; 424		
1, 0, 11			417		
			2, 2, 12; 408	2.8	3.2
			1, 0, 12; 426	8.6	10.4
			2, 0, 14		

22

powder, they found the density of Nd_2O_2Te to be 5.3 g/cc. This value, together with their x-ray diffraction data, indicated a c/a ratio of about 2, with a = 4.023 Å and c = 8.519 Å. However, these parameters lead to unreasonable values for the bond lengths in the compound, and therefore it seemed likely that the unit cell was actually larger.

In recent pycnometric measurements made at Michigan State University, a density of 7.1 g/cc was obtained for Nd_2O_2Te. The increased value indicated a c/a ratio of about 3, with a = 4.023 Å and c = 12.78 Å. These new dimensions, together with the fact that the revised Miller indices suggested a body-centered structure, led us to consider the possibility of an atomic arrangement in Nd_2O_2Te derived from the K_2NiF_4 structure, in which the rare earth atoms exhibit an unusual 9-fold coordination. Such an arrangement has been confirmed by the results of x-ray diffraction measurements on a powdered sample of Nd_2O_2Te. The relative intensities were measured with a General Electric XRD5 diffractometer using Ni-filtered Cu K_α radiation. The most probable space group is D_{4h}^{17} (I4/mmm), and the atomic positions are:

$$+ \quad (0 \quad 0 \quad 0, \quad \tfrac{1}{2} \quad \tfrac{1}{2} \quad \tfrac{1}{2})$$

Nd	0	0	z,	0	0	$\bar{z}$		in 4e
Te	0	0	0					in 2a
Ox	0	$\tfrac{1}{2}$	$\tfrac{1}{4}$,	$\tfrac{1}{2}$	0	$\tfrac{1}{4}$		in 4c

The structure was refined by using a computer program, first employed to analyze data for $LaCoO_3$ (Ref. 2), which adjusts the structure parameters to obtain a minimum value for the factor R, defined as $\Sigma|I_{obs} - I_{calc}|/\Sigma|I_{calc}|$. Application of this program gave R = 0.034 and the following values for the parameters: z = 0.341, B_{Nd} = 0.18, B_{Te} = 0.54, and B_{Ox} = 0.79, where the B parameters are atomic temperature factors. The observed and calculated intensities are compared in Table III-1, and the structure obtained is shown in Fig. III-1.
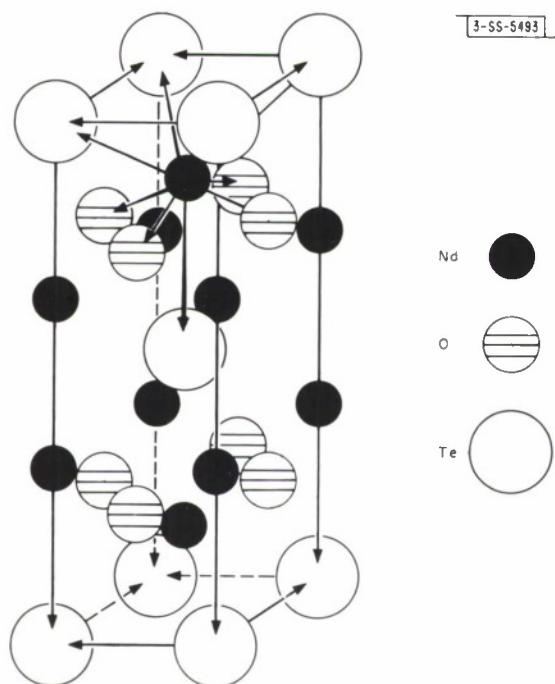

Fig. III-1. Crystal structure of Nd_2O_2Te.

The results of the present investigation indicate that x-ray powder data may be used success-fully for determining unknown crystal structures, as well as for the usual indexing and evaluation of cell parameters.

P. M. Raccah
J. M. Longo

C. NEUTRON DIFFRACTION STUDY OF ZnSe

Raccah, Arnott, and Wold[3] have recently obtained accurate relative x-ray intensity data for ZnSe by means of diffractometer measurements on powdered samples. They found systematic discrepancies between their results and the intensities calculated from theoretical atomic scatter-ing functions. These discrepancies indicate that the electron distribution differs from that given by standard theory. As suggested by Kaplan and Kleiner,[4] this difference might result because the usual scattering formulas neglect overlap terms which could be significant for a broad-band semiconductor like ZnSe, in which the electrons are quite delocalized. However, incorrect treatment of vibrational effects might also contribute to the difference between theory and experiment.

In order to investigate the role of vibrational effects, we have undertaken a neutron diffrac-tion study of ZnSe. In a non-magnetic material such as ZnSe, the neutrons will be scattered only by the nuclei, so that the standard theory involves only three potentially unknown quantities. Since the standard theory uses the same approximations to correct for vibrational effects in both neutron and x-ray diffraction, success in fitting the observed neutron intensities by op-timizing these three parameters would indicate that vibrational effects are not responsible for the inadequacy of the x-ray theory.

The M.I.T. nuclear reactor has been used to obtain several complete neutron diffraction patterns for ZnSe at room temperature and two complete patterns at liquid helium temperature. For both temperatures, analysis of the peak intensities showed a systematic departure from theory at high scattering angles. This difference presumably occurs because partial overlap of the high-angle peaks, even at liquid helium temperature where vibrational broadening should be negligible, results in overestimating the background level. An attempt to determine the back-ground by making a complete run with the sample holder empty was unsuccessful because over a third of the background originated in the sample. Therefore the data obtained so far are in-conclusive. An attempt is now being made to develop a procedure for determining the background level by analyzing the peak shapes.

K. Dwight
N. Menyuk
P. M. Raccah

D. POLYMORPHISM IN Ag_2Te AT HIGH PRESSURES AND TEMPERATURES

The polymorphism of Ag_2Te at atmospheric pressure is well known.[5,6] With increasing temperature, stoichiometric Ag_2Te is transformed successively from the low-temperature monoclinic phase into phases with face-centered cubic and body-centered cubic symmetry. In the present investigation, the phase diagram of Ag_2Te at high pressures and temperatures is being studied by means of electrical resistivity and x-ray diffraction measurements. Since these properties are sensitive to deviations from stoichiometry, the experiments are performed

on samples cut from an n-type ingot which is nearly stoichiometric, since it has a carrier concentration of only $1.0 \times 10^{17} \, \text{cm}^{-3}$.

The resistivity at hydrostatic pressures up to 16.2 kbar has been measured between room temperature and about 360°C in a piston-cylinder device which uses Dow Corning #702 silicone oil as the pressure-transmitting medium. At atmospheric pressure, in agreement with the results of Böttger and Meister[7] for a stoichiometric sample, there is an abrupt increase in resistivity at 148 ± 2°C due to the monoclinic-f.c.c. transformation. Application of pressure increases the transition temperature, as expected from the changes in volume and heat content accompanying the transformation. Table III-2 lists the transition temperatures observed in repeated runs at 5.2, 10.7, and 16.2 kbar.

TABLE III-2		
PRESSURE DEPENDENCE OF TRANSITION TEMPERATURES IN Ag_2Te		
Pressure	Temperoture of Monoclinic-to-f.c.c. Tronsition* (°C)	Temperoture of Shorp Decreose in Resistivity* (°C)
1 otm	148 ± 2	(Not obs. to 525)
5.2 kbor	188 ± 2	239
10.7 kbor	205 ± 1	260
16.2 kbar	220 ± 2	316 ± 4
* For pressures ot which more thon one meosurement wos mode, the range of observed temperotures is listed.		

At temperatures above the monoclinic-f.c.c. transformation, the resistivity at atmospheric pressure increases monotonically up to 525°C, the highest temperature investigated. (Measurements above 360°C were made with the sample in a quartz tube under argon gas.) At each of the elevated pressures, however, there is a sharp decrease in resistivity at a higher temperature, as listed in Table III-2. This decrease probably results from a transformation to a new high-pressure, high-temperature phase not observed at atmospheric pressure.

Evidence for two other high-pressure phases was obtained from measurements at room temperature under quasi-hydrostatic conditions in a tetrahedral-hinge apparatus. In several experiments, the resistivity showed a sharp increase at 21.5 − 22 kbar, then a sharp decrease of greater magnitude at 24.5 − 25 kbar, after which there was no appreciable change up to about 40 kbar, the highest pressure investigated. These observations suggest the presence of one new phase between 22 and 25 kbar, and a second above 25 kbar.

The existence of these phases has been confirmed by x-ray studies with a diamond-anvil camera of the type described by Piermarini and Weir.[8] At an average anvil pressure of about 20 kbar, the powder diagrams contain lines due to a new phase, in addition to those of the atmospheric pressure monoclinic phase. At an average anvil pressure of about 30 kbar, the lines of

the monoclinic phase are no longer observed, and additional lines appear. Since it has not been possible to index the entire set of lines obtained at this pressure, it seems likely that more than one phase is present.

The results of x-ray measurements made with a diamond-anvil camera are complicated by the existence across the anvil faces of pressure gradients whose magnitude varies with sample thickness. The magnitude of these gradients in the present camera was investigated by making x-ray measurements on finely powdered NaCl. In these experiments, the sample pressure was determined from the measured lattice constant a_o by using the compressibility of NaCl calculated by Birch.[9] An estimate for the pressure gradient was obtained from the uncertainty in a_o found by least-squares analysis, which reflects the broadness of the diffraction lines. The estimated gradients across the portion of the sample exposed to the x-ray beam were 3 and 5 kbar at average anvil pressures of 20 and 30 kbar, respectively. In addition, there was considerable variation from run to run in the sample pressure for a given average anvil pressure. Thus the sample pressure varied from 20 to 30 kbar in four runs at 20 kbar average anvil pressure, and from 24 to 44 kbar in four runs at 25 kbar average anvil pressure. These results indicate the necessity of reducing the pressure gradients in the camera in order to determine the structures of phases with narrow high-pressure stability ranges.

<div style="text-align: right">M. D. Banus
Mary C. Finn</div>

E. HIGH-PRESSURE STUDY OF MnAs

The effect of pressure in reducing the transition temperature T_c for the first-order $B8_1 \rightarrow B31$ transformation in MnAs has been reported previously.[10] It was found that above a critical pressure of 4.5 kbar the B31 phase was stable at all temperatures. It was also observed that the phase transformation was marked by an increasing degree of hysteresis as the temperature was decreased.

The pressure-temperature hysteresis curve for the reverse $B31 \rightarrow B8_1$ transformation has now been determined. The results are shown in Fig. III-2, together with those reported earlier for the $B8_1 \rightarrow B31$ transition. For temperatures down to 200°K, the hysteresis data were obtained by observing the discontinuity in resistivity due to the reverse transformation which occurred as the pressure was reduced at constant temperature. The point at atmospheric pressure and 138°K was obtained by magnetic susceptibility measurements. In this case, a specimen was converted to the B31 phase by applying 5 kbar and then cooled to 77°K. The pressure was released, the specimen was transferred without warming up to the cold stage (at 4.2°K) of a vibrating-coil magnetometer, and the magnetization was monitored as the sample was allowed to warm up to room temperature. Initially the susceptibility was small and decreased with increasing temperature, but at 138°K the magnetization increased abruptly by a factor of more than 50 to the value characteristic of the $B8_1$ phase.

The results shown in Fig. III-2, together with those obtained in an earlier study[11] of $MnAs_{1-x}P_x$, establish the following:

    (1) There is a $d\mu/dV > 0$ in the temperature interval $T_t - \Delta T < T < T_t$, where $T_t = 130°C$ is the temperature of the second-order $B31 \rightleftarrows B8_1$ transformation, $\Delta T \approx 125°C$ and μ is a manganese atomic moment. Since the thermal expansion coefficient is $\sim 2 \times 10^{-4} °C^{-1}$, this

Fig. III-2. Hysteresis of $B8_1 \rightleftarrows B31$ transition in MnAs.
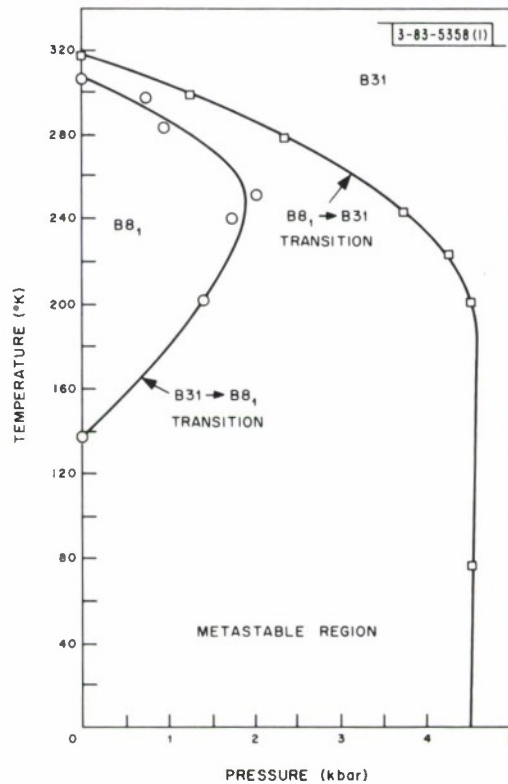
implies a $d\mu/dV > 0$ in a critical molar volume range $V_t - \Delta V < V < V_t$, where V_t is the molar volume at T_t and $\Delta V/V \approx 0.025$.

(2) A first-order $B8_1 \rightleftarrows B31$ transition at T_C occurs only if the molar volume at T_C falls within the critical range. Further, the fact that the low-temperature phase is hexagonal, with a discontinuous expansion of the basal planes on cooling through T_C, demonstrates that there is a large, positive exchange striction in the basal planes if $V > V_t - \Delta V$ at T_C. This exchange striction has essentially disappeared where $V < V_t - \Delta V$.

Bean and Rodbell[12] have shown that a first-order transition can occur at T_C if

$$T_C = T_0 \left[1 + \beta(V - V_0)/V_0 \right] \quad ,$$

both the coefficient β and the compressibility are large, and there is a large ΔV at T_C due to exchange striction. Since T_C is proportional to $W\mu*^2$, where W is the Weiss molecular field and $\mu*^2 \approx 4S(S + 1) \mu_B^2$, it follows that

$$\beta = \left(\frac{1}{W} \frac{dW}{dV} + \frac{2}{\mu*} \frac{d\mu*}{dV} \right) \quad .$$

Bean and Rodbell assumed $d\mu*/dV = 0$, and therefore required a large $dW/dV > 0$. However, analysis of available data gives $dW/dV < 0$ and

$$6 < \beta < 22 \quad \text{for} \quad 3 \geqslant (\mu_8^*/\mu_{31}^*)^2 \geqslant 2$$

27

where μ_8^* and μ_{31}^* are the atomic moments in the low-temperature $B8_1$ and the intermediate temperature B31 phases respectively. Interpretation of the first-order phase change appears to require[13] a $\beta \sim 10$.

A $d\mu/dV > 0$ requires a high-spin $\rightleftarrows$ low-spin transition in the critical molar volume interval, and hence

$$\langle d(\epsilon_{ex} - \epsilon_{cf})/dV \rangle \, \Delta V > 0.1 \, eV$$

within this interval ΔV. Here ϵ_{ex} and ϵ_{cf} are intra-atomic exchange and crystal-field splittings, respectively, and 0.1 eV is taken as the lower limit of the $\underline{d}$-band width for orbitals of e_g symmetry. Since

$$\Delta(-\epsilon_{cf}) \approx \frac{1}{3} \epsilon_{cf} \Delta V/V \approx 0.01 \, eV \quad ,$$

it follows that the sharp transition requires

$$\Delta\epsilon_{ex} = \langle d\epsilon_{ex}/dV \rangle \Delta V \geqslant 0.1 \, eV \quad .$$

Stoner[14] has pointed out that there is a maximum bandwidth, and hence a maximum overlap integral Δ_c^f for orbitals on neighboring cations, that will support spontaneous band ferromagnetism. Further, the bandwidth for bonding orbitals is greater than that for antibonding orbitals, so that $\Delta_{ab} < \Delta_b$, where the subscripts refer to antibonding and bonding orbitals, respectively. Thus the two conditions for spontaneous band ferromagnetism are

$$\Delta_b < \Delta_c^f \quad \text{and} \quad \Delta_{ab} < \Delta_c^f < \Delta_b \quad ,$$

where high-spin manganese requires the first and low-spin manganese implies the second. It is concluded that the unusual occurrence of a $d\mu/dV > 0$ over a small volume interval ΔV manifests the transition

$$\Delta_b < \Delta_c^f \rightarrow \Delta_{ab} < \Delta_c^f < \Delta_b$$

and demonstrates that Δ_c^f is quite sharply defined.

<div style="text-align: right">

J. B. Goodenough
J. A. Kafalas

</div>

F.   RETROGRADE SOLUBILITY OF Pb IN n-TYPE PbS

The solubility of Pb in PbS as a function of temperature has been investigated by means of Hall coefficient (R_H) measurements on samples annealed in argon at temperatures between 350 and 912°C and then quenched. The samples were sawed from Bridgman-grown single crystals, supplied by Battelle Memorial Institute, which contain excess Pb incorporated during their growth from undoped, nominally stoichiometric melts. For sufficiently long annealing times and sufficiently rapid quench rates, the samples obtained consist of n-type PbS saturated with dissolved Pb at the annealing temperature, together with a dispersed second phase of electrically inactive Pb microprecipitates. The measured free carrier concentration $(n = 1/eR_{77°K})$ is proportional to the concentration of excess Pb remaining in solution, since the point defects associated with the presence of Pb in excess of the stoichiometric composition are shallow donors which are completely ionized at 77°K.
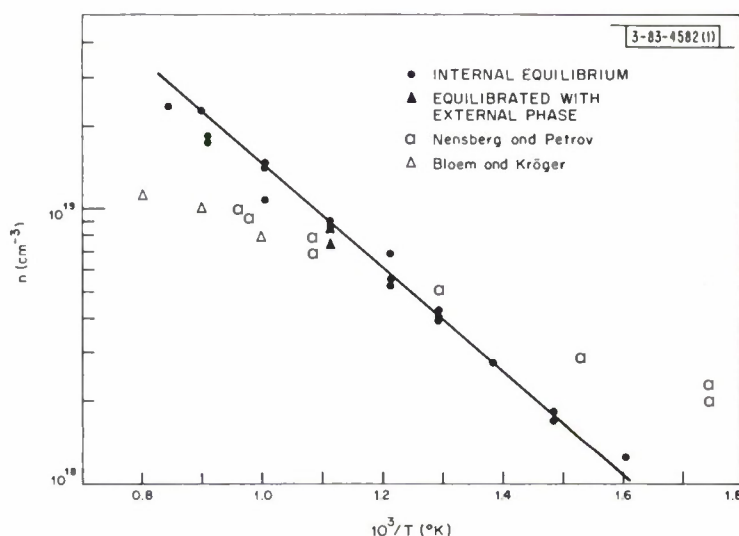
Fig. III-3. Carrier concentration (n) vs reciprocal absolute annealing temperature for n-type PbS.

The experimental results are shown in Fig. III-3, where the logarithm of carrier concentration is plotted against reciprocal absolute annealing temperature. The solubility of Pb is retrograde, since the carrier concentration decreases with decreasing temperature, from 2.4×10^{19} cm^{-3} for $1185°$K (10^3/T = 0.844) to 1.3×10^{18} cm^{-3} for $623°$K (10^3/T = 1.605). The data are well represented by the straight line shown, which corresponds to the expression $n = (1.08 \times 10^{21})$ exp$[-(4.34 \times 10^3)/T] = (1.08 \times 10^{21})$ exp$[-(0.37\,eV)/kT]$ cm^{-3}.

The two points in Fig. III-3 designated as "equilibrated with external phase" were obtained for samples which were initially converted to p-type by annealing in sulfur vapor and then saturated with Pb by equilibrating at $895°$K (10^3/T = 1.117) with a liquid-solid Pb$_{0.55}$S$_{0.45}$ mixture. The data for these samples are in good agreement with those obtained for as-grown samples annealed in argon. This result shows that the thermodynamic properties of the internal microprecipitates in the latter samples are essentially the same as those of the bulk Pb-rich external phase. Therefore it can be concluded that the straight line in Fig. III-3 gives the carrier concentrations for PbS samples lying on the Pb-saturated solidus line in equilibrium with Pb-rich liquid.

As shown in Fig. III-3, the maximum carrier concentration observed by Nensberg and Petrov[15] in recent annealing experiments similar to the present ones was only 1.0×10^{19} cm^{-3}. It seems likely that their quenching rate was not fast enough to prevent precipitation in samples annealed at the highest temperatures which they investigated. The same explanation probably accounts for the fact that the maximum carrier concentration observed by Bloem and Kröger,[16] who equilibrated PbS samples with various partial pressures of sulfur, was only 1.6×10^{19} cm^{-3}.

At lower annealing temperatures, Nensberg and Petrov[15] obtained carrier concentrations systematically higher than the present concentrations. Possibly they did not anneal long enough for their samples to reach internal equilibrium, although their annealing times would have been sufficient to equilibrate the samples used in the present experiments.

It is generally believed that the predominant point defects in Pb-rich PbS are singly ionized sulfur vacancies. If this is the case, the deviation from stoichiometry δ in $Pb_{0.5+\delta}S_{0.5-\delta}$ is equal to (1.31×10^{-23}) n, and the straight line in Fig. III-3 corresponds to $\delta = 1.41 \times 10^{-2}$ $\exp[-(0.37\,eV)/kT]$.

A. J. Strauss

G. SULFUR DONOR LEVEL IN GaSb

Single crystals of GaSb containing S concentrations of 10^{17}-10^{18} cm^{-3} have been grown from the melt by the Czochralski method. Preparation of S-doped GaSb has not been reported previously. Figure III-4 shows the temperature dependence of the Hall coefficient at atmospheric pressure for a typical n-type S-doped sample, together with data reported previously[17] for a Se-doped sample which has about the same Hall coefficient at room temperature. With decreasing temperature, the Hall coefficient of the S-doped sample increases rapidly due to donor deionization. This shows that the S donors have a finite ionization energy. In contrast, no deionization occurs for the Se-doped sample, since the lowest Se donor level is merged with the conduction band. (The small decrease in Hall coefficient with decreasing temperature observed for the Se-doped sample is due to the transfer of electrons into the lowest conduction band minimum at k = 0 from the next higher (111) minima, which at atmospheric pressure lie only $0.08 - 0.09$ eV above the k = 0 minimum.)

To determine the ionization energy of S in GaSb, computer calculations of Hall coefficient versus temperature were made for a two-conduction-band, one-donor-level model, using known parameters for the k = 0 and (111) conduction bands, and optimizing the values of donor concentration (N_D) and ionization energy (E_D). The acceptor concentration was assumed to be
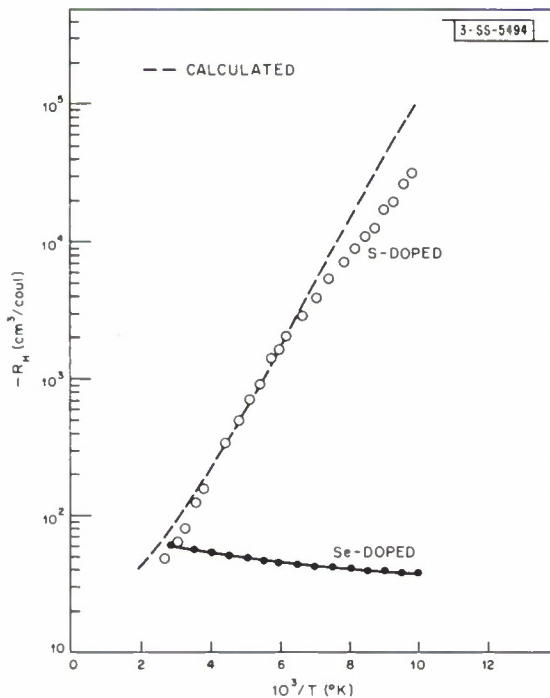

Fig. III-4. Hall coefficient (R_H) vs reciprocal temperature for n-type GaSb.

$1 \times 10^{17} \text{ cm}^{-3}$, a typical value for GaSb crystals grown from stoichiometric melts. The calculated curve best fitting the experimental results, which is shown as a dashed line in Fig. III-4, was obtained for $N_D = 7 \times 10^{17} \text{ cm}^{-3}$ and $E_D = 0.075 \text{ eV}$ relative to the $k = 0$ minimum. In an attempt to improve the fit at low temperatures, where the experimental values lie below the calculated curve, calculations were also made for the case of two S levels, the second one lying closer to the $k = 0$ band than 0.075 eV, but no improvement resulted.

The pressure dependence of room temperature resistivity for the S-doped samples has been measured by Kosicki and Paul of Harvard University, who originally suggested the preparation of S-doped GaSb. Their results, which will be reported in detail elsewhere, show that the S donor level with $E_D = 0.075 \text{ eV}$ is primarily associated with the (100) conduction band, which lies at an energy estimated to be about $0.3 - 0.4 \text{ eV}$ above the $k = 0$ minimum.[18,19] Evidence for donor levels associated with higher-lying conduction bands has been reported for CdTe, GaAs, and $GaAs_{1-x}P_x$ alloys, and evidence for a Se level in GaSb associated with the (111) minima has been presented by Bate[20] and by Kosicki and Paul.[21]

At temperatures below about 100°K, striking non-equilibrium effects are observed in resistivity and Hall coefficient measurements on S-doped GaSb. For example, when a sample is cooled rapidly from room temperature by immersing it in liquid nitrogen, the carrier concentration immediately after cooling is much higher than the equilibrium value at 77°K, frequently by more than an order of magnitude. The concentration then decreases to the equilibrium value with a time constant which depends strongly on temperature, decreasing from about 25 hours at 77°K to about 5 minutes at 90°K. Although no detailed explanation for the non-equilibrium effects has been formulated, it seems probable that the difficulty in transferring electrons from the conduction band to the donor levels results from the fact that the lowest conduction band minimum is at $k = 0$, while the donor levels are associated primarily with the (100) minima.

A. J. Strauss
G. W. Iseler

H. MAGNETORESISTANCE AND HALL COEFFICIENTS IN Ti_2O_3

Single crystal boules of Ti_2O_3 were grown using special precautions to minimize their C and N impurity content. Commercial TiO_2 and TiH_2 were mixed in appropriate amounts, outgassed at 10^{-6} torr, heated at 1100°C in an atmosphere of gettered argon, and pressed into pellets. The material was melted in a drawn molybdenum crucible under gettered argon, and single crystals with an oxygen/titanium ratio $x = 1.512$ were grown by the Czochralski technique. A V-doped single crystal was also grown from a melt containing 2 atomic-percent V_2O_3. The total cationic impurity content of the boules was of the order of 180 atomic ppm (exclusive of V), the major impurities being Si and Fe at 50 and 70 atomic ppm, respectively. The N and C concentrations were 1800 and 240 atomic ppm, respectively.

The magnetoresistance $\Delta\rho/\rho_o$ and Hall coefficient R of these crystals were measured at the National Magnet Laboratory in magnetic fields H up to 218 kG. As shown in Table III-3 and Fig. III-5, the undoped Ti_2O_3 samples exhibited anisotropy in ρ and $\Delta\rho/\rho_o$. For current at a 45° angle between the c axis and basal plane of the corundum structure, magnetoresistance values exceeding 3.4 were attained at 4.2°K and H = 218 kG, without any indication of saturation

TABLE III-3 RESISTIVITY AND HALL COEFFICIENT OF Ti_2O_3						
Direction of Current Flow	Resistivity (ohm−cm)			Holl Coefficient (cm^3/coul)		
	4.2°K	77°K	300°K	4.2°K	77°K	300°K
Undoped Ti_2O_3 (somple 115)						
$\perp$ c axis	17, 22	4.9×10^{-2}	−	+1.9 − +3.0	−	−
45° to c axis	25, 35	0.13	0.085	+4.8	−	+0.031
‖ c oxis	68	0.13	0.018	+0.84 − +2.4	+0.165	+0.032
V-doped Ti_2O_3 (somple 110-111)						
‖ o oxis	$8.3 \times 10^{-4*}$	8.5×10^{-4}	9.7×10^{-4}	+0.0080	+0.0040	+0.0035
‖ c oxis	9.5×10^{-4}	9.7×10^{-4}	−	+0.0045	+0.0043	−
‖ b oxis	1.2×10^{-3}	1.2×10^{-3}	1.4×10^{-3}	+0.0040	+0.0045	+0.0039

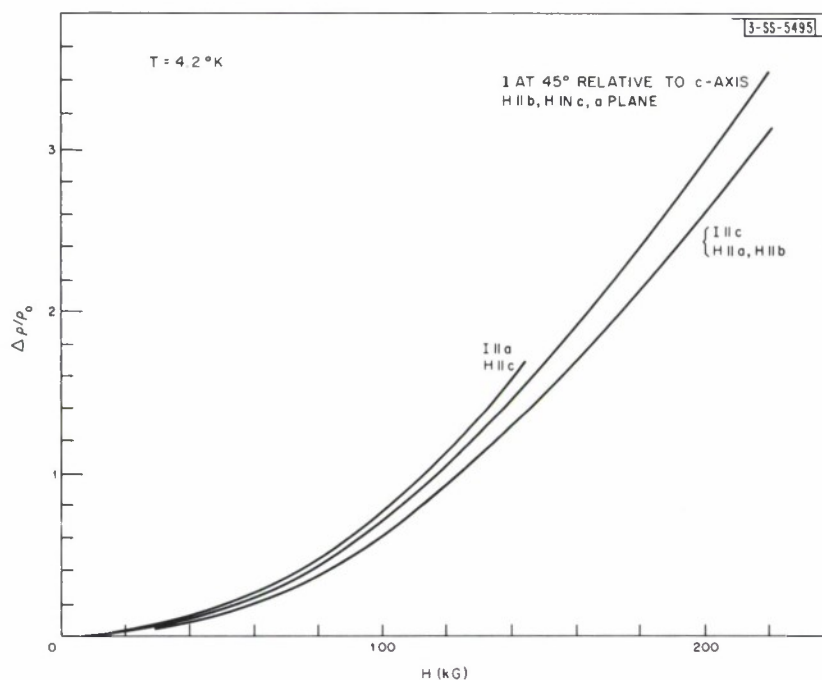* in the limit of high magnetic field. As $H \rightarrow O$, $R \rightarrow +0.028$.

Fig. III-5. Magnetoresistance at 4.2°K in undoped Ti_2O_3 (sample 115), with current flow
(I) and magnetic field (H) along specified crystallographic directions.

effects. This confirms earlier results[22] which led to the conclusion that the conduction prop-
erties of Ti_2O_3 at 4.2°K cannot be interpreted in terms of a conventional one-band transport
mechanism. At 77°K, the magnetoresistance was barely measurable; this suggests that a sig-
nificant change in conduction properties occurs between 4.2 and 77°K. The strong temperature
dependence of resistivity is noteworthy.

The resistivity and magnetoresistance of V-doped Ti_2O_3 are shown in Table III-3 and
Fig. III-6. In contrast to the undoped material, $\Delta\rho/\rho_0$ is negative; ρ remains reasonably iso-
tropic, almost independent of temperature, and quite small. With the present sample the nega-
tive magnetoresistance effects at 4.2°K are more pronounced than in the V-doped specimens
studied earlier,[23] which contained greater concentrations of N and C. The anisotropy effects
in the magnetoresistance are also marked. At 77°K, the negative magnetoresistance, though
small, is still detectable: $\Delta\rho/\rho_0 = -3.5 \times 10^{-3}$ at H = 218 kG.

The Hall coefficient of the undoped material was positive and small in magnitude; it could
be determined only with great difficulty because the true Hall voltage amounted to less than
0.3 percent of the total transverse voltage across the probes. In the V-doped material, which
had essentially no spurious transverse voltages, the Hall coefficient was easily measurable;
R was again positive and nearly independent of H. The values obtained correspond to a carrier
concentration of about 1.5×10^{21} holes/cm^3 on a one-band model.

The origin of the p-type behavior of the V-doped samples has not been firmly established;
this effect could be due to deviations of sample composition from stoichiometry. In one sample

33
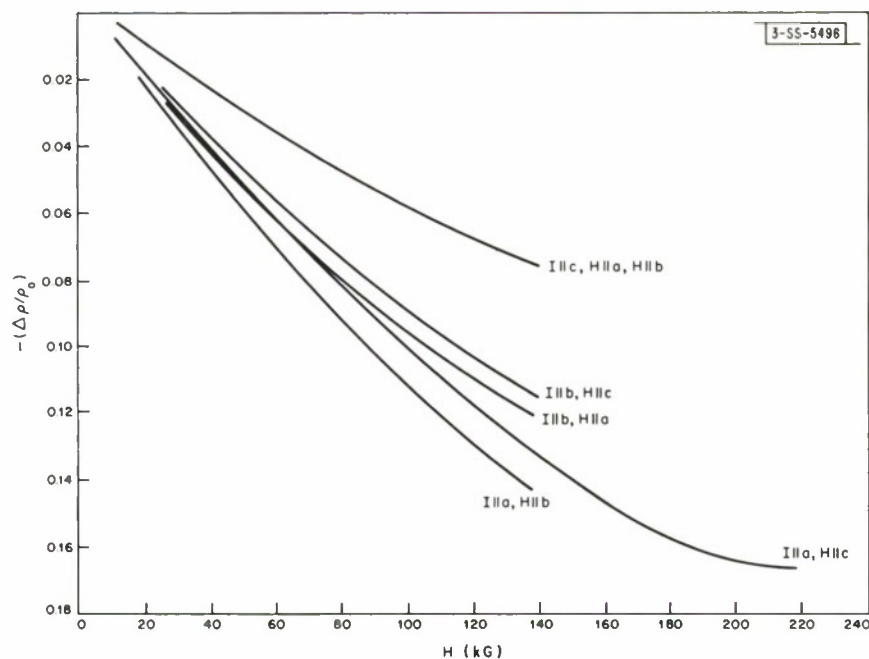
Fig. III-6. Negative magnetoresistance at 4.2°K in V-doped Ti_2O_3 (sample 110-111), with current flow (I) and magnetic field (H) along specified crystallographic directions.

(not used in the investigations reported here) the stoichiometry ratio x in $Ti_{1-y}V_yO_x$ was found to lie in the range 1.517 to 1.527. This lends credence to a recent suggestion[24] that part of the V in the crystal may be present in the quadrivalent state, which would require the incorporation of excess oxygen into the lattice. The concentration of acceptors due to the presence of excess oxygen in the above-mentioned sample would exceed the concentration of electrons introduced by the substitution of V for Ti, thereby rendering the material p-type. Furthermore, the quadrivalent V is also associated with a magnetic moment; as outlined previously[23] this is required to explain the negative magnetoresistance effects.

J. M. Honig   R. E. Fahey
T. B. Reed   L. L. VanZandt

I.   UNUSUAL CRYSTAL-FIELD ENERGY LEVELS AND EFFICIENT LASER PROPERTIES OF YVO_4:Nd

Optical absorption and laser studies have been made on single crystals of YVO_4 grown from iridium crucibles in an oxyhydrogen gas-fired furnace by a modified Czochralski technique.[*] This compound crystallizes in a D_{4h}, tetragonal space group of the zircon $(ZrSiO_4)$ type. All rare earth vanadates have the same structure and form solid solutions with YVO_4. Therefore, it will be possible to investigate a variety of cross-pumped laser systems, as in the case of yttrium aluminum garnet (YAG).[25]

---

* These crystals were supplied by H. M. Dess and S. R. Bolin of the Linde Division, Union Carbide Corporation.

Fig. III-7. Absorption levels of Nd^{+3}-doped YAG and YVO_4 between 0.6 and 1.0 μ measured at 300°K for samples 3 mm thick. Fine structure represents transitions from excited levels of ground state. Numbers below absorptions represent the Stark split levels. For YAG:Nd and YVO_4:Nd, splitting corresponds to tetragonal and cubic symmetry respectively.
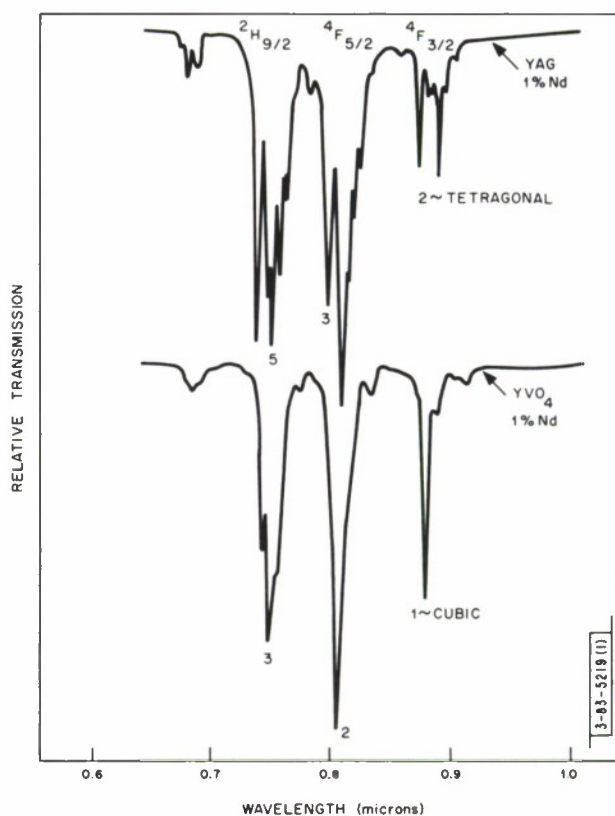
At present, Nd^{+3}-doped YAG is one of the most efficient solid state lasers. Figure III-7 compares the absorption spectrum of Nd^{+3}-doped YAG and YVO_4. The Nd^{+3} absorptions are labeled according to free ion, R-S coupling. Koningstein and Geusic[26] have shown these term designations are appropriate for YAG:Nd.* For this case the Nd^{+3} ion is situated at a tetragonal site. The tetragonal distortion, although weak, is sufficient to completely remove the $(J + 1/2)$-fold degeneracy and produces a pronounced splitting of the $^4F_{3/2}$, $^4F_{5/2}$, and $^2H_{9/2}$ levels shown in Fig. III-7.

In contrast, very little Stark splitting is observed for Nd^{+3} in YVO_4. This reduction in splitting is apparent in the absorption spectrum of Fig. III-7 (where the resolution is greater than $10\,cm^{-1}$). It is present throughout the visible spectrum and persists at low temperatures. The reduction is also shown by the fluorescence spectrum for YVO_4:Nd, which contains only half the lines present in the YAG:Nd spectrum. Most of the emission in YVO_4:Nd occurs at $1.069\,\mu$ in a line whose halfwidth is ~5 Å at 77°K. Consistent with the reduced splitting, the ^4F metastable level of YVO_4:Nd has an oscillator strength larger and a radiative lifetime (33 μsec) smaller, by a factor of about 7, than for YAG:Nd.

---

* As a result of detailed crystal-field calculations these authors have shown that Nd^{+3} in YAG is at a site of tetragonal symmetry.
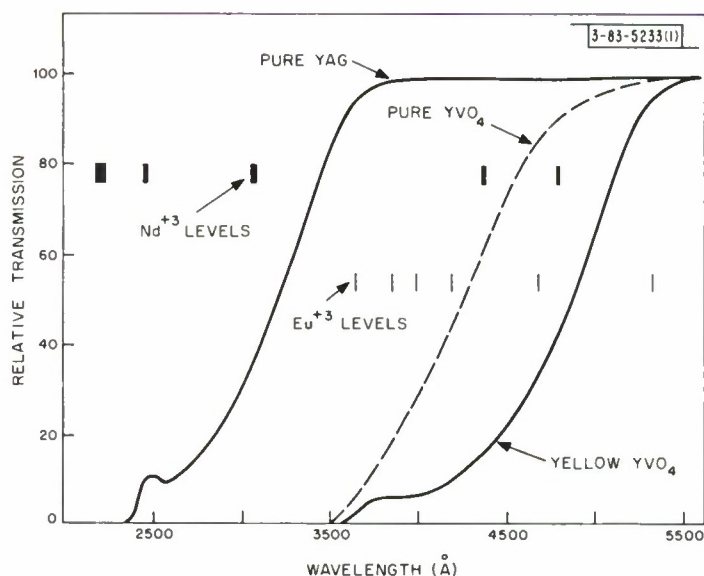
Fig. III-8. Relative transmission of YAG and YVO$_4$ from 2000 to 5500 Å. Spectra were measured at 300°K for samples 3 mm thick. Absorption levels of Nd^{+3} and Eu^{+3} are also shown.

Figure III-8 shows the relative transmission of YAG and two types of YVO$_4$. "Pure" YVO$_4$ has a normal absorption edge and is colorless. Photons of wavelength below 4500 Å cause it to fluoresce in several lines between 4800 and 5750 Å, as previously reported by Brixner and Abramson.[27] This emission is completely quenched in YVO$_4$:Nd at 300°K due to energy transfer from the lattice to the Nd^{+3} ions. Only partial quenching occurs at 77°K. This implies that the energy transfer processes are phonon assisted. No evidence for energy transfer has been reported for YAG:Nd.

A second type of YVO$_4$ has a broad absorption peaking near 4200 Å and is yellow. Samples of each type are being investigated by electron spin resonance in order to detect the possible presence and site symmetry of V^{+4} (3d^1) ions. The pulsed laser threshold is lower in the yellow material than in the colorless. Therefore the additional absorption at 3500-5000 Å in the yellow type also transfers energy to the Nd^{+3} ions.

Low pulsed laser thresholds (~1J) have been obtained in YVO$_4$:Nd^{+3}. The low threshold is due to: (1) the reduced Stark splitting, and, (2) the substantial transfer of lattice energy to the Nd ions.

J. R. O'Connor

J.   ELECTRON MICROPROBE ANALYSIS

A method has been developed for the determination of Pb and Sn in Pb$_{1-x}$Sn$_x$Te alloys by electron microprobe analysis. Simultaneous x-ray intensity measurements of the fifth order Lα_1 line of Pb(λ = 1.175 Å) and the third order Lα_1 line of Sn(λ = 3.600 Å) are made on separate spectrometers. Several areas of each alloy sample are examined. Intensity measurements of the Pb and Sn lines are also made on pieces of PbTe and SnTe, respectively, which are used as standards.

TABLE III-4 ANALYSIS OF $Pb_{1-x}Sn_xTe$ ALLOYS					
Microprobe Analysis (mole fraction)			Wet Chemical Analysis (mole fraction)		
PbTe	SnTe	Total	PbTe	SnTe	Total
0.968	0.031	0.999	0.986	0.017	1.003
0.943	0.062	1.005	0.940	0.057	0.997
0.799	0.207	1.006	0.797	0.206	1.003
0.620	0.378	0.998	0.608	0.385	1.003

Calibration curves for Pb and Sn in the $Pb_{1-x}Sn_xTe$ system were calculated by using the backscattered electron correction of Duncumb and Shields,[28] the ionization correction of Nelms,[29] and the absorption correction of Philibert.[30] The mole fraction of PbTe present in each sample is obtained from the calculated curve using the ratio of the Pb line in the sample to that in PbTe. Similarly, the mole fraction of SnTe is obtained from the ratio of the intensity of the Sn in the sample to that in SnTe.

Four samples analyzed with the microprobe were also analyzed for Pb and Sn by wet chemical techniques.[31] The amounts of PbTe and SnTe were calculated from the analyses assuming each element to be present entirely as the telluride. The results obtained by both methods are given in Table III-4. They are in good agreement except for the low Sn sample where the error in both types of analysis is large.

Mary C. Finn

REFERENCES

1. R.A. Kent and H.A. Eick, Inorg. Chem. 1, 956 (1962).

2. P.M. Raccah and J.B. Goodenough, Phys. Rev. (to be published).

3. P.M. Raccah, R.J. Arnott, and A. Wold, Phys. Rev. 148, 904 (1966).

4. T.A. Kaplan and W.H. Kleiner, private communication.

5. J.F. Rowland and L.G. Berry, Amer. Min. 36, 417 (1951).

6. A.J. Frueh, Jr., Amer. Min. 46, 659 (1961).

7. O. Böttger and W. Meister, Ann. Physik 9, 367 (1962).

8. G.J. Piermarini and C.E. Weir, J. Res. Natl. Bur. Std. 66A, 325 (1962).

9. F. Birch, J. Geophys. Res. 57, 227 (1952).

10. Solid State Research Report, Lincoln Laboratory, M.I.T. (1966:3), p. 17, DDC 641498.

11. J.B. Goodenough, D.H. Ridgley, and W.A. Newman, Proc. Int. Conf. on Magnetism (Nottingham, 1964) p. 542.

12. C.P. Bean and D.S. Rodbell, Phys. Rev. 126, 104 (1962).

13. R.W. DeBlois and D.S. Rodbell, Phys. Rev. 130, 1347 (1963).

14. E.C. Stoner, Phil. Mag. 25, 899 (1938).

15. Y.D. Nensberg and A.V. Petrov, Inorg. Mater. 1, 1365 (1965).

16. J. Bloem and F.A. Kröger, Z. Physik. Chem. 7, 1 (1956).

17. A.J. Strauss, Phys. Rev. 121, 1078 (1961).

18. H. Ehrenreich, J. Appl. Phys. 32, 2155 (1961).

19. W. Paul, J. Appl. Phys. 32, 2082 (1961).

20. R.T. Bate, J. Appl. Phys. 33, 26 (1962).

21. B.B. Kosicki and W. Paul, Phys. Rev. Letters 17, 246 (1966).

22. Solid State Research Report, Lincoln Laboratory, M.I.T. (1966:1), p. 25, DDC 632998.

23. Ref. 10, p. 18.

24. J.B. Goodenough, private communication.

25. Z.F. Kiss and R.C. Duncan, Appl. Phys. Letters 5, 200 (1964); L.F. Johnson, J.E. Geusic and L.G. Van Uitert, Appl. Phys. Letters 8, 200 (1966).

26. J.A. Koningstein and J.E. Geusic, Phys. Rev. 136, A711 (1964).

27. L.H. Brixner and E. Abramson, J. Electrochem. Soc. 112, 70 (1965).

28. P. Duncumb and P.K. Shields, Proceedings of the Electron Microprobe Symposium (John Wiley and Sons, Inc., New York, 1966), p. 284.

29. A.T. Nelms, NBS Circular 577 (1956) and Supplement (1958).

30. J. Philibert, Proceedings of the Third International Symposium on X-ray Optics and X-ray Microanalysis (Academic Press, Inc., New York, 1964), p. 379.

31. Ref. 10, p. 23.

IV. PHYSICS OF SOLIDS

A. ELECTRONIC BAND STRUCTURE

1. Current Pulse Modulated Reflectivity of Metals

The current pulse modulated reflectivity technique reported in the last Solid State Research Report (1966:3, p. 26), has been applied to the study of gold and nickel. The d-band metals are of particular interest since, even though there exist in the literature[1] considerable optical as well as photoemission results, the interpretations of these measurements in terms of band structure is not yet conclusive.

Films, of the order of 2000 Å thick, of gold and nickel were evaporated onto 0.150 mm thick glass substrates; the substrates were cemented to a liquid nitrogen cooled heat sink with silicone grease which, for improvement of its thermal conductivity, was mixed with silver powder. Electrical leads were silver-cemented to the samples. The current pulse rate was about 15 Hz, with a unit duty cycle, and the peak power dissipated in the samples was about 12 watts/cm^2; this power dissipation raised the temperature of the film an average of about 40°K above the base temperature which was near 77°K. The modulation of the temperature at 15 Hz was of the order of a few degrees. The rest of the system was conventional.

The results obtained for $\Delta R/R$ on the gold and nickel films are shown in Figs. IV-1 and IV-2 along with the reflectivity R of the same films. The curves, particularly the results for gold, show well defined structure out to 10 eV, this being the first time modulation measurements have extended into the vacuum ultraviolet. For gold, the results below 5 eV are similar to those of Garfinkel et al.,[2] who used the piezoreflectivity method.

Although a detailed analysis and interpretation of the measurements is not possible at this time, a few points concerning the results can be made. For gold, one of the most notable features of the data is the sharp dispersion-like shape around 2.5 eV which is only 0.1 eV wide from the minimum in the curve to the maximum. In this region the behavior of the dielectric constant and optical properties is the result of both free electron behavior and interband transitions. The onset of interband transitions is what prevents the reflectivity from dropping below 33 percent in this region. Since the free electron contribution to the reflectivity and dielectric constant

$$\epsilon^f = 1 - \omega_p^2/[\omega(\omega + i/\tau_c)] \quad , \tag{1}$$

where ω_p is the plasma frequency, depends on the scattering time τ_c, any modulation of this parameter is likely to show in a $\Delta R/R$ measurement. It seems possible then that the initial sharp structure around 2.5 eV may be due not only to the onset of $L_{32} \rightarrow L_2$ transitions previously reported[3] but also to the modulation of τ_c. This sharp structure is absent in nickel because the onset of interband transitions in this metal occurs at a much lower energy than in gold; thus the free electron effects which cause the sharp drop in the reflectivity in gold are masked in nickel.

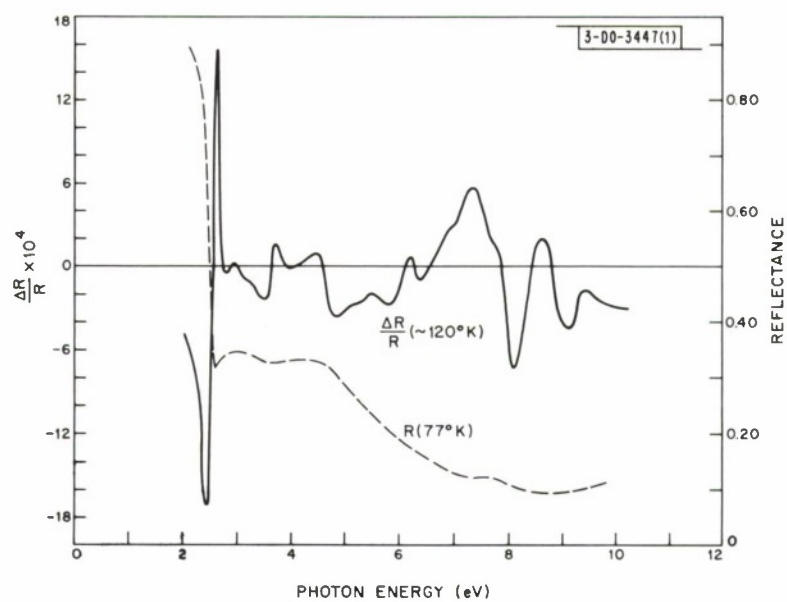Fig. IV-1. Current modulated reflectance ΔR/R and reflectance
R for gold films from 2 to 10 eV.

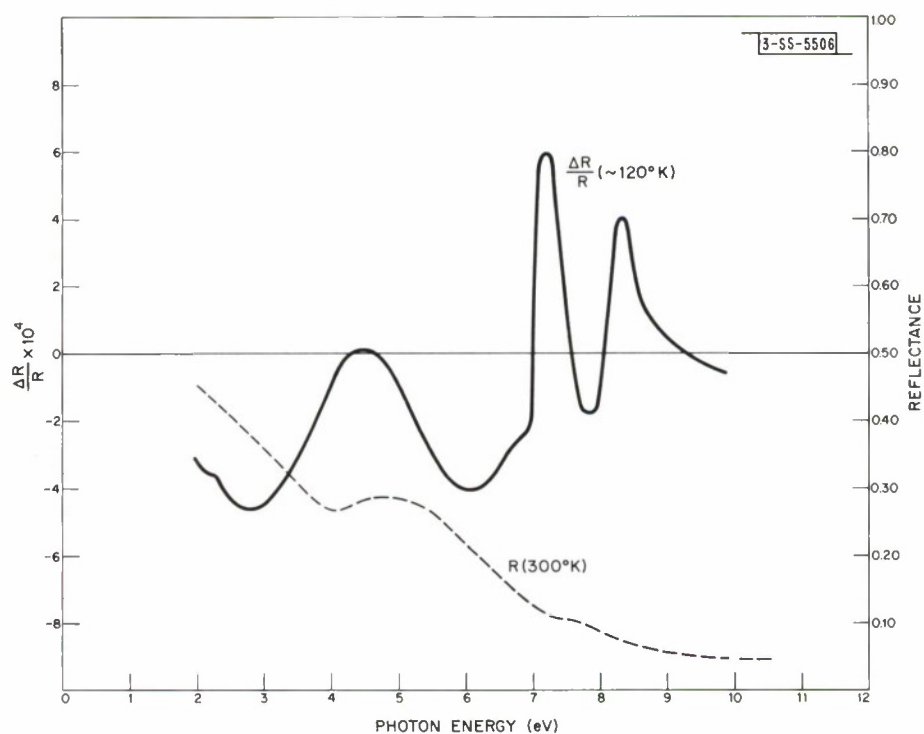Fig. IV-2. Current modulated reflectance ΔR/R and reflectance R for nickel
films from 2 to 10 eV.

All the previous papers[3] concerned with the optical properties and band structure of d-band metals have neglected any effects of spin-orbit interaction. For the atomic state, the d electron spin-orbit energy is of the order of 1.8 eV for gold and about 0.3 eV for nickel.[4] Although it has not been calculated, a splitting of this order could also be expected for the solids and should be evident in the $\Delta R/R$ spectrum.

Finally, it appears from photoemission studies on copper, silver and nickel,[5] that direct transitions in d band metals may not be the only source of absorption. Evidence suggests that for many transitions, only the electronic density of states is important and that $\vec{k}$ conservation is unimportant. The relative importance of direct and indirect transitions is thus in question[1] so it appears that the interpretation of optical data is not unambiguous at this time. Nevertheless, it is hoped that information and data obtained from new, more sensitive, experimental methods, such as the differential optical measurements, may help the theorist in calculating the energy bands of solids. The results presented here using current modulation indicate that much more structure is present in the optical properties of gold and nickel than one would have believed from the relatively uncomplicated reflectivity spectra.

W. J. Scouler
J. Feinleib

2. Current Pulse Modulated Magnetoreflectivity in InSb*

In addition to using the electroreflectivity and current pulse modulated reflectivity techniques for studying metals and semiconductors, we have examined their use for investigating magnetic phenomena in semiconductors. We have found that the current pulse, or thermal modulation, appears well suited for studying magneto-oscillations in the differential reflectivity near the direct band edge in InSb cooled to liquid nitrogen temperatures. Under these conditions, with a peak modulation power of 0.5 watt and a magnetic field of 100 kG, magneto-oscillations are observed across the energy gap from near 0.225 eV up to about 0.8 eV with excellent signal-to-noise ratio and $\Delta R/R \sim 10^{-3}$. These oscillations correspond very closely with the principal oscillations observed in magnetoabsorption, as well as with theoretical predictions. Further optimization of the technique is needed before we can determine the relative merit of this method for investigating new materials.

J. Feinleib
S. H. Groves
C. Pidgeon†

3. Magnetoreflection Experiments in Arsenic*

Oscillations in the magnetoreflectivity of single crystal arsenic have been observed at low temperatures, with the magnetic field $\vec{H} \| \vec{S}$, where $\vec{S}$ is the Poynting vector. These are the first experimental observations in arsenic at infrared frequencies, and provide information on certain energy bands lying within 0.5 eV of the Fermi energy. With $H \|$ trigonal axis, oscillations have been observed only in the energy range $0.185 < \hbar\omega < 0.375$ eV, and they have been

---

identified with interband transitions across an energy gap of 0.175 eV and a reduced effective cyclotron mass of 0.015 m$_o$. These oscillations are of exceptionally large amplitude, even larger than the corresponding effect in bismuth. Nonparabolic behavior is found for the energy bands associated with this interband transition.

With H$\|$ binary axis, smaller amplitude oscillations are observed in the energy range $0.366 < \hbar\omega < 0.7$ eV. These oscillations are identified with interband transitions across a band gap of 0.346 eV. Since these oscillations vanish for the polarization $\vec{E}\|$ bisectrix axis, the energy band extrema are expected to be located at a high symmetry point in the Brillouin zone. The relation of these results to recent DHVA measurements,[6] and to the Lin-Falicov band model[7] is being investigated.

M.S. Maltz[*]
S. Fischler[†]
M.S. Dresselhaus

4. Optical Studies of Sulfur-Doped Silicon

The following is an abstract of a paper which was presented at the International Conference on the Physics of Semi-conductors at Kyoto, Japan, in September, 1966, and which is to be published in the Journal of the Physical Society of Japan, vol. 21 (1966). This work is a continuation of that last reported on page 55 of Solid State Research Report (1965:2).

Sulfur, a Group VI element, is a mono- or divalent donor in silicon. We find that it gives rise to at least four different impurity centers, with ionization energies ranging from 0.1 to 0.6 eV. Two of these centers (at low temperatures) are singly ionized[8] and two are neutral. The spacings and the polarization dependence of the intensities are well described in the simple one-valley effective mass approximation for transitions which are hydrogenic p-like in this approximation. The singly ionized centers have an effective nuclear charge of +2, and therefore the spacings of the transitions to the p-like levels are four times as large as for the neutral centers.[9] There are, however, observed features not predicted in the simple effective mass approximation, and some of these will be discussed. One is a splitting of the $2p_o$-like levels in the ionized centers. In addition to the p-like transitions, lines have also been observed which we attribute to transitions from the ground state to the many-valley orbital triplet levels (s-like transitions).

The study of these centers under a calibrated uniaxial stress gives much information. The behavior of the p-like transitions for all 4 centers gives directly the same value of the pure shear deformation potential[10] of the conduction band, $E_2 = 7.9$ eV. The behavior of the s-like transitions with stress is characterized by deformation potentials which are much smaller than the band edge value.

[*] Electrical Engineering Department, M.I.T.

[†] Present address: NASA, Cambridge.

The stress dependence helps considerably in the identification of many of the transitions. For three of the centers, splittings are observed which are not due to shifts of the conduction band minima, but which appear to be a result of the non-tetrahedral symmetry of the center. It is expected that the uniaxial stress measurements will enable the site symmetry of all four centers to be identified.

One of the centers does appear to have a tetrahedral symmetry. For this center we have observed a pair of very sharp absorption lines, separated by approximately 0.3 meV, which are believed to represent transitions to the orbital triplet level split by spin-orbit coupling. The shift and splitting of the transitions with stress and the absorption intensities with polarized light are in reasonable agreement with such an interpretation.

W. E. Krag   H. J. Zeiger
W. H. Kleiner   S. Fischler[*]

5. Observation of Polaron Effects on the Intraband Magnetoabsorption of InSb

In the continuing study of polaron effects, it has been found theoretically that the polaron cyclotron energy, $\hbar\omega_c$, is a discontinuous function of magnetic field[11] near the LO phonon energy, $\hbar\omega_o$, at least when α, the electron-LO phonon coupling constant, is small. Above $\hbar\omega_o$, $\hbar\omega_e$ is predicted to jump in energy by an amount $\approx \alpha \hbar\omega_o$ when compared to the value obtained by extrapolation of the low-field plot of $\hbar\omega_e$. In addition, for $\hbar\omega_c \approx \hbar\omega_o$, the occurrence of an electron-lattice resonance condition shifts the n = 1 Landau level strongly, as predicted from theory and observed previously in the _interband_ magnetoabsorption.[12] We have examined the _intraband_ magnetoabsorption of n-type InSb for photon energies from 4 to 26 meV. Our results clearly show the offset $\alpha \hbar\omega_o$ as well as the beginning of the large effects reported earlier[12] for $\hbar\omega_c \approx \hbar\omega_o$. We also observe absorption lines associated with donor states, which show polaron effects. This work constitutes additional experimental confirmation of predicted polaron effects in InSb and provides an estimate of the coupling constant α.

D. H. Dickey
E. J. Johnson
D. M. Larsen

6. Pressure Experiments on HgSe, HgTe and $HgSe_xTe_{1-x}$ Alloys[†]

Experimental results on the pressure variation of the thermoelectric power, α, for n-type HgSe, HgTe and $HgSe_xTe_{1-x}$ alloys have been reported[13] which show that with increasing pressure $|\alpha|$ increases for HgSe and decreases for HgTe. If the samples studied were indeed extrinsic these results give information about the energy level ordering at $\vec{k} = 0$, in particular that

$E(\Gamma_6) > E(\Gamma_8)$ for HgSe and $E(\Gamma_8) > E(\Gamma_6)$ for HgTe. As stated in the earlier report,[13] this result for HgSe was unexpected.

At this point in this incomplete investigation, two new results of pressure experiments should be reported. From the first result it is concluded that experimental data are needed to establish whether or not the samples previously used were extrinsic. From the second result, which is obtained from an optical pressure experiment, it is suggested that the ordering $E(\Gamma_8) > E(\Gamma_6)$ is appropriate for HgSe; this conclusion is opposite to that obtained from thermoelectric power measurements.

In the first of these experiments, thermoelectric power vs pressure measurements were made on HgSe samples with electron concentrations between 5×10^{17} and 3×10^{18} cm^{-3}. Since the last report a measurement of the Hall coefficient vs pressure for a sample of HgSe with 5×10^{17} electrons/cm^3 has shown a change of 10 percent in 6 kilobars. For this concentration, then, the extrinsic condition, which would give a zero Hall coefficient change with pressure, does not hold. Piotrzkowski et al.[14] claim that the Hall coefficient is independent of pressure for their HgTe, with 1×10^{18} electrons/cm^3, which shows a decrease of $|\alpha|$ with pressure. This is about the heaviest doping of HgSe for which a definite change of α with pressure can be detected. Thus, a comparison of the Hall coefficient vs pressure behavior for HgSe and HgTe with 1×10^{18} cm^{-3} carriers is at least necessary before there can be confidence in the simple interpretation of the thermo-electric power vs pressure results.

The second pressure experiment has been performed by Dr. W. M. DeMeis of Harvard. He has measured the pressure dependence of the absorption edge in heavily doped n-type HgSe and HgTe (the absorption edge corresponds to transitions from the top of the valence band to the Fermi level in the conduction band). The results for both materials can be explained by assuming a pressure coefficient of 12×10^{-6} eV/bar for the $\Gamma_6 - \Gamma_8$ energy gap and the energy ordering $E(\Gamma_8) > E(\Gamma_6)$. The pressure coefficient of this gap is empirically known to fall in the range 9 to 15×10^{-6} eV/bar for the diamond and zinc blende semiconductors. If, on the other hand, HgSe has the ordering $E(\Gamma_6) > E(\Gamma_8)$ and a valance band maximum not at $\vec{k} = 0$, then a pressure coefficient about half of that given above is needed to obtain a zero or negative thermal energy gap; this falls outside the usual range of coefficients for this gap. Although the results of this experiment, then, do not conclusively establish the ordering of levels at $\vec{k} = 0$ in HgSe, they add to the list of indirect evidence which favors the $E(\Gamma_8) > E(\Gamma_6)$ band structure.

S. H. Groves

7. Analysis of Shubnikov-de Haas Results for HgSe

Whitsett[15] has made a thorough experimental study of the Shubnikov-de Haas (SdH) effect in n-type HgSe. An important first result of his work is that the stoichiometry of HgSe can be varied to give 1×10^{17} to 5×10^{18} homogeneously distributed electrons per cm^3. Thus, it is probably the best n-type zinc blende material in which to study the SdH effect.

Secondly, by measuring the temperature dependence of the oscillation amplitudes, Whitsett found the effective mass at the Fermi level for various concentrations and was able to assign values to the two parameters which are most important for the conduction band curvature: $|E(\Gamma_8) - E(\Gamma_6)|$ and the momentum matrix element P between these states.

Thirdly, Whitsett showed that the SdH oscillation period was only weakly dependent upon crystal orientation with respect to magnetic field direction, as expected for a conduction band located at $\vec{k} = 0$. However, a beat frequency was observed in the higher concentration samples, and for the magnetic field in the (110) plane, the beating was found for all directions except for $\vec{H} \parallel \langle 110 \rangle$. A nearly spherical Fermi surface with bulges in the $\langle 111 \rangle$ directions was proposed by Whitsett to qualitatively explain the beating behavior. For the magnetic field in the $\langle 111 \rangle$ or $\langle 100 \rangle$ directions, for example, this Fermi surface has a maximum area off $k_3 = 0$ and a local minimum in the area at $k_3 = 0$, where k_3 is parallel to the direction of the magnetic field. These two external areas give rise to two SdH frequencies which add together in the conductivity to give an average frequency term modulated by a beat frequency term $[\sin A + \sin B = 2 \sin \frac{1}{2} (A + B) \cos \frac{1}{2} (A - B)]$. For the magnetic field in the $\langle 110 \rangle$ directions, on the other hand, the cross sectional area has only a maximum at $k_3 = 0$ and a minimum of zero area when the k_3 component of the energy equals the Fermi energy, thus giving rise to only one SdH frequency.

Although Whitsett's model qualitatively explains the SdH behavior of HgSe, apparently no attempt has been made until now to compare it with the Fermi surface constructed from the theoretical E vs k expressions for small gap zinc blende materials such as those derived by Kane[16] for InSb. The expression found by Kane for either a Γ_6 or Γ_8 conduction band is the following

$$E^{\pm} = E' + \frac{\hbar^2 k^2}{2m_o} + a^2 A' k^2 + b^2 [Mk^2 + (L - M - N) f_1(k)]$$

$$+ c^2 [L'k^2 - 2(L - M - N) f_1(k)] \pm \sqrt{2} abB f_2(k) \tag{2}$$

where

$$f_1(k) = (k_x^2 k_y^2 + k_x^2 k_z^2 + k_y^2 k_z^2)/k^2$$

and

$$f_2(k) = [k^2(k_x^2 k_y^2 + k_x^2 k_z^2 + k_y^2 k_z^2) - 9k_x^2 k_y^2 k_z^2]^{1/2}/k \quad .$$

E' is the conduction band eigenvalue which results from the diagonalization of the Hamiltonian between the s-like (Γ_6) and p-like ($\Gamma_8 + \Gamma_7$) basis which includes the k · p and the largest spin-orbit interaction terms. a, b and c are the normalized coefficients which give the admixture of s and p state basis in the eigenvector corresponding to E' · A', L, M, N, L' and B are parameters which are determined by the interaction between the higher conduction bands and the s and p bands.

It is convenient to separate Eq. (2) into three parts: The first, which includes E', is spherically symmetric. It is the predominant part of the energy and gives the non-parabolic shape of the band but does not contribute directly to the beating effects. The second part of the expression adds warping to the energy surface and can be written $(b^2 - 2c^2) (L - M - N) f_1(k)$. The combination $(b^2 - 2c^2) (L - M - N)$ contains opposing contributions from the k · p matrix element between the p-like components of the conduction band and the higher Γ_{15} and Γ_{12} conduction bands. The Γ_{12} band is thought to be considerably higher in energy than the Γ_{15} and because

of an energy difference denominator in $(L - M - N)$, the interaction with Γ_{15} gives the predominant contribution. The sign and directional dependence of this term are such that they result in the deviation from spherical symmetry that is required by the Whitsett model. The last part of the energy expression consists of the $\pm B$ term above, and, in the case of a Γ_8 band, a term linear in k which is not shown in Eq. (2). For the region of k-space of interest to us this linear k term has the same orientation dependence as the B term. These contributions to the energy arise from the lack of inversion symmetry in the zinc blende lattice and, consequently, are zero in the diamond lattice materials. They have been given theoretical attention but as far as we know there have been no experimental determinations of their size.

We have used the following procedure to calculate cross sectional areas for a sample of given carrier concentration: First, complete degeneracy and spherical symmetry are assumed to find the radius of the Fermi sphere, k_F, from the carrier concentration. Then the spherically symmetric part of Eq. (2) is used to find the Fermi energy E_F by a numerical diagonalization of the interaction matrix for $k = k_F$, a spin-orbit splitting of 0.5 eV, and Whitsett's two parameters $|E(\Gamma_8) - E(\Gamma_6)| = 0.24$ eV and $P = 7.2 \times 10^{-8}$ cV-cm. This process also gives the coefficients a, b, c at $k = k_F$. Then, the full expression in Eq. (2) with E_F on the left-hand side is used to find the magnitude of the k vector k_r which balances the equation for k in a given direction. Finally, the integration $\frac{1}{2} \int_0^{2\pi} k_r^2(\varphi) \, d\varphi$ gives the cross sectional area for φ in the plane of interest.

The results of the cross sectional area computation are the following: the quantity $(L - M - N)$ must be at least three times as big in HgSe as in Ge and InSb for a Γ_8 conduction band, and six times as big for a Γ_6 conduction band, to explain the beating by the second part of Eq. (2), or the Whitsett Fermi surface. Only when $(L - M - N)$ is made this large does the cross sectional area off $k_3 = 0$, for k_3 aligned to one of the $\langle 100 \rangle$ crystal areas for example, become greater than the area at $k_3 = 0$. Our knowledge of the position of the Γ_{15} conduction band — the quantity which largely determines the size of $(L - M - N)$ — comes from weak structure in the high energy reflectivity, which is tentatively identified with Γ_8 to Γ_{15} optical transitions.[17] From this data the values of 3.05, 3.45 and 5.2 eV have been assigned to the $\Gamma_8 - \Gamma_{15}$ energy separation in Ge, InSb and HgSe, respectively. For $L - M - N$ to be large enough to explain the beating, the $\Gamma_8 - \Gamma_{15}$ energy gap would have to be ~ 1 eV for HgSe for a Γ_8 conduction band and even less for a Γ_6 conduction band. Therefore, from what is known about the higher bands, the warping does not seem sufficient to cause the beating. In addition, with the warping large enough to produce beating, the average or high frequency SdH oscillation shows a much stronger dependence on magnetic field direction than was observed by Whitsett.

With this result, the third part of Eq. (2) must be examined as a potential source of the beating. We find that the difference in areas corresponding to the zinc blende-splitting of a Γ_8 conduction band can give the observed frequencies for $\vec{H} \| \langle 111 \rangle$ if B is 5 to 10 units of $\hbar^2/2m_0$ in magnitude. This is not unreasonable when compared to theoretical estimates. B has to be ten times as large if the conduction band is Γ_6. For the magnetic field in a $\langle 111 \rangle$ direction the Fermi surfaces corresponding to the split bands do not touch at $k_3 = 0$. For $\vec{H} \| \langle 100 \rangle$ there are four $\langle 100 \rangle$ directions in the $k_3 = 0$ plane where the surfaces touch and for $\vec{H} \| \langle 110 \rangle$ the $k_3 = 0$ plane includes two $\langle 100 \rangle$ directions and four $\langle 111 \rangle$ directions where the surfaces

touch. However, the Whitsett data require that beating be present for $\vec{H} \parallel \langle 100 \rangle$ but not for $\vec{H} \parallel \langle 110 \rangle$. It is not yet clear what areas should be used in these directions or even if this semiclassical approach is valid for calculation of the SdH frequencies. Unfortunately, the quantum-mechanical calculation of the magnetic energy levels including all the terms in Eq. (2) is a difficult computational task. Bell and Rodgers[18] have recently performed such a computation for one direction of magnetic field in InSb in which the magnetic interaction Hamiltonian matrix of infinite order is truncated to a 250×250 matrix. We are currently looking for a simpler treatment which can explain qualitatively the orientational dependence of the beating.

It is interesting that the beating effects have not been observed in gray tin samples with concentrations comparable to those of HgSe.[19] Gray tin has the Γ_8 conduction band which enhances the warping part of Eq. (2) but has diamond symmetry so that there is no zero field splitting of the two-fold degeneracy. Most other zinc blende materials in which the SdH effect can be observed have Γ_6 rather than Γ_8 conduction bands. HgTe is an exception but the highly doped material we have studied so far is not sufficiently homogeneous to give reproducible beating patterns.

It is a pleasure to acknowledge P. Trent for suggestions on several of the computations used in this work.

S. H. Groves
P. W. Wyatt*

8. Conductivity Calculations for Bismuth

Using the density matrix formalism,[20] we have calculated the zero field conductivity of bismuth assuming a) the holes may be treated as free particles with an anisotropic effective mass, b) the electrons may be treated by the two-band model of Lax,[21] Cohen and Blount,[22] c) the velocity matrix elements for the electrons are those calculated by Wolff[23] based on the two-band model of Lax, Cohen and Blount. The reflectivity and transmission curves calculated from this conductivity are found to agree quite well with the curves for transmission displayed by Boyle and Brailsford[24] and Boyle and Rodgers[25] and the absorptance curve of Nanney.[26] This calculation also confirms the idea that the major contribution to the "core dielectric constant" comes from the electrons.

This density matrix technique is now being applied to obtain a detailed line shape of the magnetoreflection in bismuth, using the magnetic energy levels of the two-band model and the field and frequency dependent velocity matrix elements given by the calculation of Wolff.

M. S. Maltz†
M. S. Dresselhaus

9. Fourier Expansion for Energy Bands in Silicon

Using the Fourier expansion scheme reported earlier (Solid State Research Report 1966:2, p. 42), the energy bands and frequency dependent dielectric constant have been calculated for

---

*Present Address: Yale University.

†Electrical Engineering Department, M.I.T.
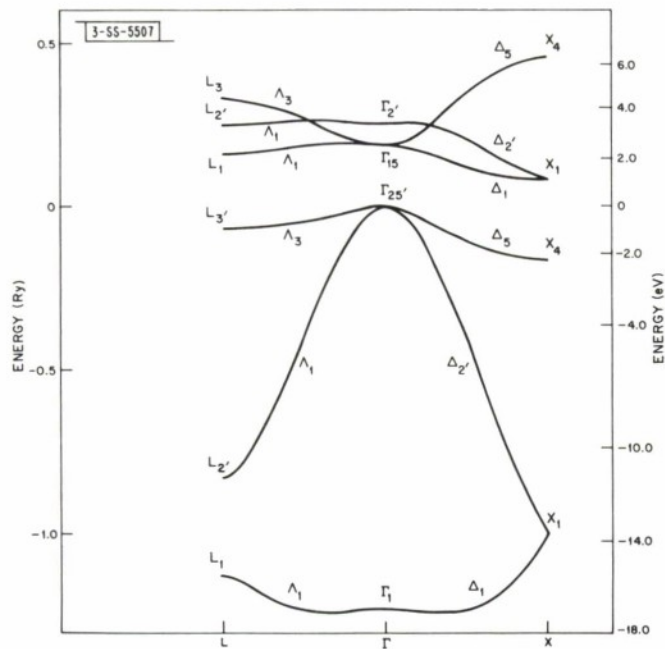
3-SS-5507

Fig. IV-3. Energy bands of silicon calculated by means of Fourier expansion scheme; energy band parameters have been determined from experimental values of energy gaps and effective masses.
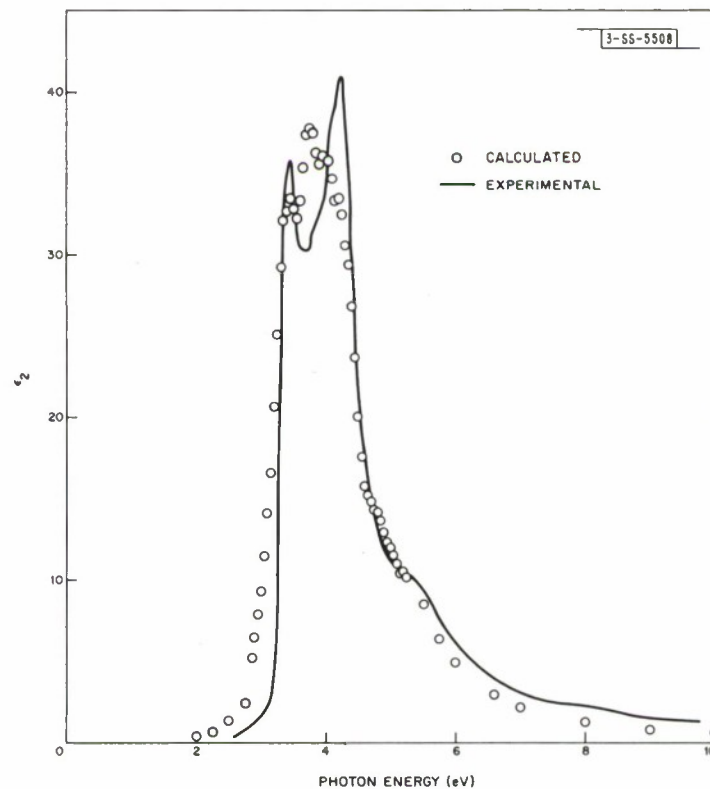
3-SS-5508

O CALCULATED

—— EXPERIMENTAL

Fig. IV-4. Comparison between calculated and experimental variation of ϵ_2, the imaginary part of the dielectric constant in silicon.

silicon. The band parameters are determined exclusively from experiment. The calculation of the dielectric constant proved extremely useful in the identification of observed experimental structure with characteristic features of the electronic structure. The silicon energy bands are shown in Fig. IV-3 and the dielectric constant calculated for these bands is shown in Fig. IV-4. For comparison, the experimental dielectric constant of Philip and Ehrenreich[27] is also shown in Fig. IV-4.

<div align="right">G. Dresselhaus
M. S. Dresselhaus</div>

B. MAGNETISM

1. High Temperature Expansions for the Classical Heisenberg Model. I. Spin Correlation Function

The following is an abstract of a paper submitted for publication (see also Ref. 28).

The diagrammatic representation of the first eight coefficients in a high-temperature series expansion of the zero-field spin correlation function $\langle S_f \cdot S_g \rangle_\beta$ is presented for any range of exchange interaction and for any lattice. The present calculation exploits the order-of-magnitude simplifications which occur in treating the quantum-mechanical spin operators in the Heisenberg model as isotropically-interacting classical vectors of length $[S(S + 1)]^{1/2}$. This classical approximation — "the classical Heisenberg model" — appears to be excellent in the critical region, $T \cong T_c$, for values of the spin quantum number $S > 1/2$. The utility of the high-temperature series for $\langle S_f \cdot S_g \rangle$ is discussed: Besides providing an efficient method of obtaining the high-temperature expansions for all the thermodynamic functions together, it contains additional physical information. Such applications of the high-temperature series expansion for $\langle S_f \cdot S_g \rangle_\beta$ will be treated in subsequent papers.

<div align="right">H. E. Stanley</div>

2. High Temperature Expansions for the Classical Heisenberg Model. II. Zero-Field Susceptibility

Any extension of the high-temperature expansion of the zero-field susceptibility

$$\chi/\chi_{Curie} = 1 + \sum_{\ell=1}^{\infty} a_\ell (J/kT)^\ell \tag{3}$$

seems to be highly impractical because of the enormous labor involved.* Nevertheless, there exists a considerable need for more terms. Recently Stanley and Kaplan (SK)[31] showed that order-of-magnitude simplifications occur when one treats the non-commuting quantum-mechanical

---

* "The labor of calculating just one more term in the series is considerably greater than the labor of calculating all the previous terms" [P. J. Wood, thesis, King's College, Newcastle-upon-Tyne, 1958 (unpublished)]. The series for general spin S seems limited to the six terms calculated by Rushbrooke and Wood.[29] Recently nine terms (ten for the loose-packed lattices) have been obtained for S = 1/2 by methods practicable only for S = 1/2, 1 (Ref. 30).

TABLE IV-1

THE SUSCEPTIBILITY COEFFICIENTS a_ℓ

ℓ	Honeycomb Net	Square	Triangular	Simple Cubic	Body-Centered Cubic	Face-Centered Cubic
1	2.0000	2.6667	4.0000	4.0000	5.3333	8.0000
2	2.6667	5.3333	13.3333	13.3333	24.8889	58.6667
3	3.02222	9.9556	39.8222	43.3778	114.7259	413.8667
4	3.3185	16.9086	110.6963	136.2963	509.7877	2,855.3481
5	3.6797	27.2404	292.3096	424.5446	2,249.9706	19,415.8527
6	3.5759	42.2122	741.8552	1,301.5034	9,779.9445	130,694.4263
7	2.8846	63.0670	1,822.0514	3,967.8674	42,335.1558	873,209.9634
8	2.6796	91.6638		11,998.0391	181,758.3614	5,800,796.3979

spin operators occurring in the Heisenberg Hamiltonian $\mathcal{H} = -\Sigma_{ij} J_{ij} S_i \cdot S_j$ as commuting vectors of length $[S(S + 1)]^{1/2}$, suggesting that many more terms in the series can be obtained "classically" than "quantum-mechanically." Moreover, SK argued that useful results could be obtained from this classical Heisenberg model or "infinite spin approximation," since errors are small and decrease rapidly with S. For example, the errors in the extrapolated estimates of $T_c/S(S + 1)$ for cubic lattices are only ~4 percent for S = 1 and ~1 percent for S = 5/2.[*] Our purpose here is to present the results of a calculation of the first eight terms (seven terms for close-packed lattices) in the high-temperature series, Eq. (3), for a Heisenberg Hamiltonian with nearest-neighbor interactions only.[†] The $a_\ell(\ell \leq 8)$ are obtained directly from the first eight coefficients α_ℓ^{fg} in the corresponding high-temperature series expansion for the zero-field static spin correlation function[‡]

$$\langle S_f \cdot S_g \rangle_\beta = \sum_{\ell=0}^\infty \frac{(-1)^\ell}{\ell!} \alpha_\ell^{fg} \beta^\ell \tag{4}$$

by means of the relation

$$a_\ell = [X\ell! (-J)^\ell N]^{-1} \sum_{fg} \alpha_\ell^{fg} \tag{5}$$

where $X \equiv S(S + 1)$ and $\alpha_\ell^{fg} = \Sigma_{\bar{d}} \alpha_\ell^{fg}(\bar{d})$. The utility of the diagrammatic representations is that $\alpha_\ell^{fg}(\bar{d})$ depends only upon the topology of the diagram $\bar{d}$, and not upon the angles between the lines. Thus for a given order ℓ one need calculate only the different $\alpha_\ell^{fg}(\tau)$ where τ indexes the topological type of diagrams $\bar{d}$. Although there are many different topological types of diagrams with ℓ straight lines and one wavy line which might potentially contribute to α_ℓ^{fg}, SK showed that $\alpha_\ell^{fg}(\tau)$ is zero for a large majority of these types. Thus the summation $\Sigma_{fg} \alpha_\ell^{fg}(\bar{d})$ in Eq. (5) may be replaced by $\Sigma_{\tau=1}^{t_\ell} \alpha_\ell^{fg}(\tau) \Lambda(\tau)$, and the non-zero $\alpha_\ell^{fg}(\tau)$ are given (for $\ell < 8$) in Tables I through IV of Ref. 28. Here t_ℓ denotes the number of different topological types of diagrams contributing to order ℓ, and $\Lambda(\tau)$ denotes the number of occurrences of the diagram $\bar{d}$ of topological type τ, e.g., the number of four-sided polygons which can be placed on a square lattice is N; the number of hexagons, 3N.

In this fashion we calculated the a_ℓ for $\ell = 1, 2, \ldots, 8$ in terms of basic "lattice constants," which in turn have been tabulated for the more common two- and three-dimensional lattices.[34] The "general lattice" expressions are too lengthy to include here, so we instead present, in Table IV-1, the a_ℓ for three three-dimensional (fcc, bcc, and s.c.) lattices, and for three two-dimensional (triangular, square, and honeycomb) lattices.

---

[*] The errors in the extrapolated estimates of $T_c/S(S + 1)$ for the common two-dimensional lattices are much larger, since here $T_c(2)/S(S + 1) \sim 2 - 1/S(S + 1)$ (Ref. 32).

[†] Eight terms for the fcc, bcc, and s.c. lattices have recently been published by Wood and Rushbrooke.[33] Our general-lattice results agree with their calculation when we specialize to the three cubic lattices they considered.

[‡] The diagrammatic representation of the first eight terms a_ℓ^{fg} in the high-temperature series expansion of the spin correlation function $\langle S_f \cdot S_g \rangle_\beta$ have been obtained recently.[28]
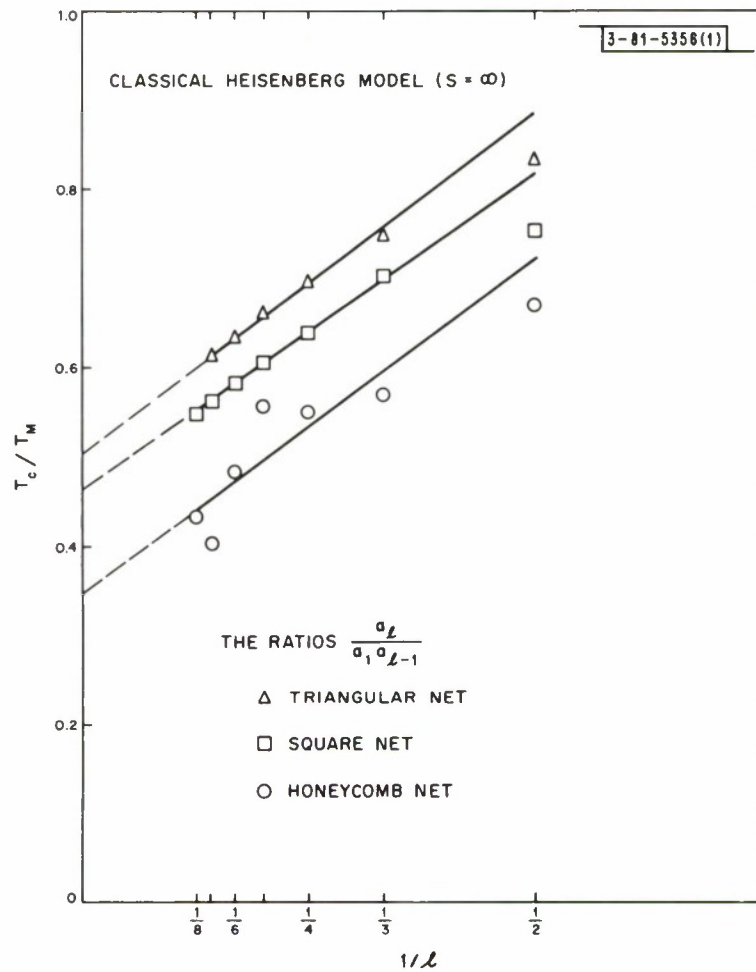
Fig. IV-5. The ratios of $a_\ell / a_1 a_{\ell-1}$ of successive terms in the susceptibility series for the honeycomb, square, and triangular planar lattices.

It is perhaps not amiss to consider here the effect of the additional terms upon two hotly-debated physical questions:* First, does a phase transition exist in the two-dimensional Heisenberg model with nearest-neighbor ferromagnetic interactions? The classical Heisenberg model is of particular interest in connection with this question because it presents the same "dilemma" as that which occurs quantum-mechanically: Arguments plausible at low temperatures lead to a magnetization which is infinite in one and in two dimensions,[37] whereas the high-temperature expansion coefficients strongly suggest a phase transition at a non-zero temperature in two as well as in three dimensions (but not in one).[35] It was recently pointed out that for some two-dimensional lattices the ratios $a_\ell/a_{\ell-1}$ of successive terms in the high temperature series expansion Eq. (3), when plotted against $1/\ell$, seem to approach a straight line for large ℓ in a manner which is as regular as for three-dimensional cases.[32] Hence the extrapolation to $\ell = \infty$ and the identification of the intercept with a critical temperature T_c can be made as reliably in two dimensions as in three. In Fig. IV-5 we plot the ratios $a_\ell/a_1 a_{\ell-1}$ against $1/\ell$ for the classical Heisenberg model. The additional terms in these classical cases strengthen the conclusion, already drawn from the first six terms, that there probably is a phase transition for the two-dimensional classical Heisenberg model.

The second question is, does the critical exponent γ in the assumed form of the divergence of χ, $\chi \sim (T - T_c)^{-\gamma}$ as $T \to T_c^+$, have the value 4/3 for the fcc, bcc, and s.c. lattices? Previous arguments for $\gamma = 4/3$ have been based upon the assumption that the more classical the model, the more rapidly the terms of the high-temperature series settle into a smooth behavior. This assumption, coupled with the observation from the first six terms that $\gamma(S = \infty) = 4/3$, has led to the proposal that $\gamma = 4/3$ independent of spin and lattice. Recently it was suggested that this proposal is false,[36] there being instead a slow but nevertheless clear variation of γ with S. On the basis of the six terms available for general S, no variation with lattice within the class of fcc, bcc, and s.c. was detected.† With the aid of the additional terms now available for $S = \infty$, it is possible to detect a variation with lattice as well: for the classical Heisenberg model, $\gamma = 1.33 \pm 0.01$ for the fcc lattice, with $\gamma = 1.355 \pm 0.01$ for the bcc and s.c. lattices. This new result is based upon the comparatively straightforward and simple "slope method" for determining the value of γ: If χ does diverge as $T \to T_c^+$ with a power law, then for large ℓ, $a_\ell/a_1 a_{\ell-1} = (T_c/T_M) [1 + (\gamma - 1)/\ell]$, where T_M is the ordering temperature predicted by molecular field theory. The slopes of the straight-line extrapolations in Fig. IV-6 for the fcc, bcc, and s.c. lattices yield the values of γ given above.

H. E. Stanley

3. Possible Phase Transition for Two-Dimensional Heisenberg Models

The following is an abstract of a paper which was presented at the 12th Annual Conference on Magnetism and Magnetic Materials, Washington, D. C. and which has been accepted for publication.[35]
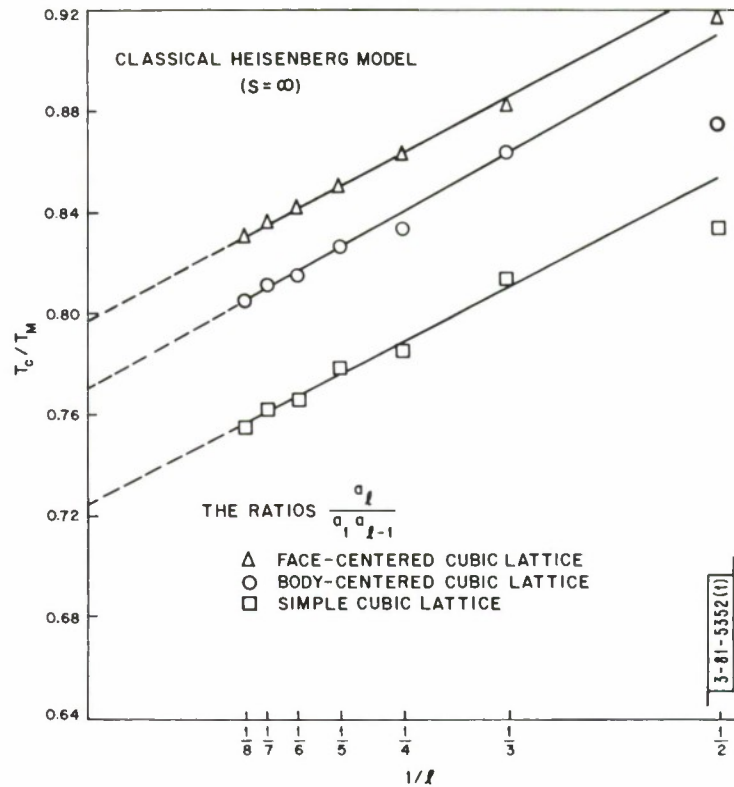

Fig. IV-6. The ratios $a_\ell / a_1 a_{\ell-1}$ of successive terms in the susceptibility series for the simple, body-centered, and face-centered cubic lattices.

Recently the authors presented evidence suggesting the presence of a phase transition for two-dimensional Heisenberg models with nearest-neighbor ferromagnetic interactions and $S > \frac{1}{2}$. Here we further analyze the first six coefficients of the high-temperature series for the zero-field susceptibility, and incorporate the results of recent calculations beyond sixth order into the arguments for a phase transition. It is found that the higher order coefficients support the previous suggestion concerning the existence of a phase transition for $S > \frac{1}{2}$, and are consistent with a zero critical temperature for the particular case $S = \frac{1}{2}$. Finally, two preliminary calculations on the nature of the low-temperature phase are described. The first of these, due to F. J. Dyson, is an intuitive generalization of spin wave theory. The other is an approximate calculation for the rectangular net within the classical Heisenberg model: Considering this net to consist of linear chains, the intra-chain interactions are treated exactly, while the inter-chain interactions are treated via a molecular field approximation. Both of these calculations support the original suggestion of a phase transition for two-dimensional Heisenberg models.

H. E. Stanley
T. A. Kaplan

54

4. Zero Sound and Plasma Oscillations

The properties of spin sound, the propagation of waves of spin density, in unmagnetized or weakly magnetized Fermi gases have been studied in the time dependent Hartree-Fock approximation. The results have been reported previously (Solid State Research Report 1965:3, p. 49) and will appear in Physical Review. Two results of particular interest were the discovery of a short wavelength cutoff to the spectrum of the oscillations and a demonstration that portions of the spectrum which were Landau damped, (that is, where single fermions were able to absorb spin waves in energy and momentum conserving processes), nonetheless should produce experimentally observable resonances, indeed, of no greater linewidth than portions not suffering from Landau damping.

As a sequel to this, the properties of density oscillations, ordinary zero sound, have been studied in the same approximation. When the fermions interact through Coulombic repulsive forces, as do electrons, we recover the well known plasmon dispersion equation. In addition, we have found an additional branch of the density oscillation spectrum in this approximation, a set of roots to the well known dispersion equation which has been heretofore neglected. The oscillations of this second branch are Landau damped, but because they occur at low frequency and with a phase velocity very near the Fermi velocity, they, like the Landau damped spin sound modes, could lead to experimentally observable resonances. The short wavelength cutoff is also characteristic of density oscillations. In a dense Coulomb gas, the cutoff occurs at a frequency above the limits of definition of the modes and is hence only a mathematical quirk. A Fermi gas with short range interparticle forces, however, offers some possibilities for observing the cutoff at relatively lower frequencies where the entire spectrum is well defined. The spectrum has been studied using parameters of the interactions appropriate to liquid He^3. The results of this work have been submitted for publication.

L. L. VanZandt

C. TRANSPORT THEORY

1. Transport Theory of Interacting Electrons in the Random Phase Approximation

In order to study the influence of the electron-electron interaction on the transport properties of the conduction electrons in a metal, we have considered the model of an interacting electron gas driven by an external electromagnetic field and scattered by randomly distributed impurities. As a first step for a systematic many-body theory of this problem, we treat the electron-electron interaction in the random phase approximation, which is valid for sufficiently high electron density. Thus this theory includes all the plasma (collective) effects on the electromagnetic properties.

We have considered both longitudinal and transverse external electromagnetic fields. We express the linear response of the system in terms of the average total electromagnetic field, by constructing a generalized kinetic equation. To achieve this we have made use of the technique we developed earlier[38] for the case of non-interacting electrons. This kinetic equation for the impurity-averaged density matrix is valid for arbitrary frequencies of the external field

and for a general one-electron Hamiltonian. In addition, the effects of the electron-impurity interaction are described without any approximation. The Born approximation for the scattering is easily derived.

The effects of the electron-electron interaction appear in various ways. First, the impurity potential is screened by the gas in thermal equilibrium, i.e., statically, and the external field is screened by the dielectric constant at the driving frequency. Additional terms describe the modification of the scattering and interference terms of the transport equation.

We have so far examined the consequences of this theory for the special case of the homogeneous electron gas in the Born approximation for the scattering and for a homogeneous driving field. For $\omega = 0$ we have found that the simple minded picture of an independent electron (quasi-particle) driven by the average total field and scattered by a statically screened impurity is valid. For $\omega \neq 0$ this is no longer true; effects of the dynamic screening of the impurities begin to come in. For $\omega\tau \gg 1$, where τ = relaxation time, again the model of an independent electron is valid but now with the impurity potential screened by the geometric mean of the dielectric constants at frequencies zero and ω. This latter description is a very simple expression of the results of various theories[39] for this particular case. We should point out that these theories[39] are not only restricted to the case of uniform fields, but are also unsatisfactory in that the identification of the total field is incomplete. At least for the longitudinal case they give the correct result through the cancellation of two errors.

<div align="right">P. N. Argyres</div>

2. Landau Theory of a Fermi Liquid in Random Impurities

The transport theory for the Landau quasi-particle distribution function in the presence of random impurities is incomplete. Strictly speaking it is valid only for $\omega = 0$, where ω is the frequency of an external driving field, and approximately correct for $\omega\tau \ll 1$, where τ is a measure of the relaxation time. For $\omega\tau \gg 1$, a region of experimental interest, it is incorrect. Furthermore, the "memory" effects of the collision processes have been ignored. We have begun to examine the possibility of a new approach to this problem that would allow us to derive a transport equation for the quasi-particle distribution function for arbitrary ω, subject only to the usual restriction of the existence of the quasi-particle. The essence of the approach is to treat the quasi-particle as a quantum-mechanical particle and derive first its "Schrodinger equation" and then its transport equation.

<div align="right">P. N. Argyres
J. Sigel*</div>

D. SCATTERING EXPERIMENTS WITH LASERS

1. Stimulated Brillouin and Raman Scattering in Quartz Between 2.1 and 293°K

Further results on stimulated Brillouin scattering experiments in quartz at 2.1°K have lent additional support to the contention that the anomalous Brillouin shifts reported by Krivokhizha[40] et al. were misinterpreted and are actually due to intense stimulated Raman radiation which sets

---

* Physics Department, M.I.T.

in at low temperatures. We had previously observed a weak additional line in radiation scattered out of the x-direction which, because of its relative displacement (3 percent) with respect to successive interference orders of the etalon, was inferred to be the 466 cm^{-1} Raman line of quartz (see Fig. IV-7).

In scattering along the z-axis, we observe a shift (with or without the regular Brillouin shift appearing) which is compatible with the 128 cm^{-1} Raman line of quartz (see Fig. IV-8). Since interferometer measurements cannot uniquely identify widely shifted lines, we simultaneously photographed the scattered radiation on a grating spectrograph. In every case the suspected Raman lines were observed and showed complete correlation with the unidentified Fabry-Perot etalon lines. For example, the spectrogram taken simultaneously with the interferometer picture of Fig. IV-8 shows only a strong line at 132 cm^{-1} and no other lines. Thus the subsidiary line in Fig. IV-8 is identified as "128 cm^{-1}" stimulated vibration of the classical room temperature Raman spectrum (duly temperature shifted). Consequently, at 2.1°K, for z-directed scattering, the Raman threshold for the 128 cm^{-1} line is lower than that for the 466 cm^{-1} line; for x-directed scattering both the 466 cm^{-1} and 128 cm^{-1} line often appear. In all cases the stimulated Raman radiation is sufficiently intense to pass through the narrow-band ruby-pass filter in front of the etalon. There seems to be a tendency for stimulated Brillouin scattering to be suppressed at the expense of stimulated Raman radiation. Such interference between Brillouin and Raman processes has been observed previously.[41]

In order to verify that additional nonlinear effects did not set in at higher powers, we raised the power incident on the sample in small increments. The measured results continued to be the same up to 100 Mw, at which point catastrophic failure of the helium dewar occurred.

Thus it appears that the anomalous Brillouin shifts reported in Ref. 40 can be attributed to stimulated Raman scattering, which becomes quite strong at low temperatures.[*] This phase of the experiment has been completed, and the results have been submitted to Science.

P. E. Tannenwald
J. B. Thaxter
F. H. Perry

2. Temperature Dependence, Orientation Correlation, and Molecular Fields in Second Harmonic Light Scattering from Liquids and Gases

The following is an abstract of a paper which is being prepared for publication.

The properties of second harmonic light scattering in fluids are derived in terms of the molecular polarizabilities, orientation correlation among molecules, and the electric field F_α in the unilluminated liquid. Measurements of scattering intensity in CCl_4 and water, from about 10°C to 60°C, are reported. The variations with temperature, and therefore apparently the effects of changes of orientation correlation, are slight. The influence on the scattering

---

[*] The appearance of Raman lines on the Fabry-Perot interferogram enables us to measure Raman shifts and their temperature dependences to an accuracy of 0.1 cm^{-1}.
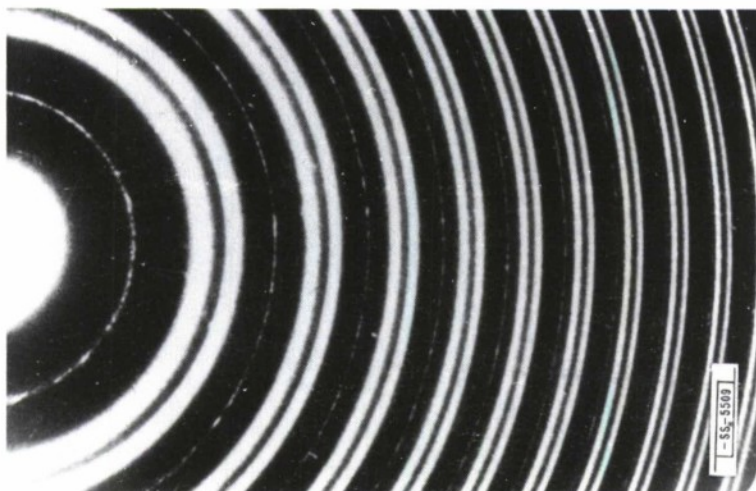
Fig. IV-7. Fabry-Perot interferometer spectrum of backward Brillouin scattering along x-direction in quartz at 2.1°K. Brillouin shift is 0.84 cm^{-1}. The weak line is displaced successively by 0.11 cm^{-1} with respect to each interorder spacing and is identified to be the 468 cm^{-1} Raman line.

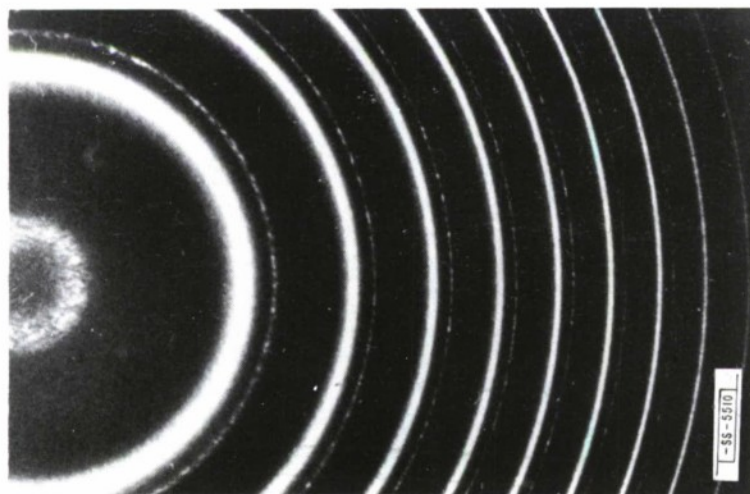

Fig. IV-8. Backward Brillouin scattering along z-direction in quartz at 2.1°K. No Brillouin shift. The weak line indicates an apparent Brillouin shift of 2.30 cm^{-1}, but is actually the 132 cm^{-1} Raman line.

of preferred orientation in CCl_4, of the type deduced from X-ray diffraction, is calculated. The third rank molecular polarizability tensor consists of the fourth rank polarizability contracted with F_α, in addition to the term previously known, which is independent of F_α. With F_α arising from molecular multipole moments, the new term explains some experimental depolarizations in liquids, and accounts for most of the line, but not the background, observed in methane gas. In the case of molecular dipole moments, it can cause spectral narrowing.

D. L. Weinberg

3. The Raman Spectrum of GaS and GaSe

We have observed the Raman spectrum of GaS and GaSe using $6328 \overset{\circ}{A}$ and $1.06\,\mu$ lasers. The first order spectrum for each compound consists of five lines, which occur for GaS at 69.6, 183.9, 285.7, 289.3 and $357.6\,cm^{-1}$, and for GaSe at 59.6, 133.8, 209.5, 253.8 and $308.6\,cm^{-1}$. These compounds are layer structures in which the layers are relatively weakly bound to each other. Each layer has D_{3h} point group symmetry and contributes four atoms per unit cell. The stacking of layers in GaS, and one modification of GaSe, retains the D_{3h} symmetry and results in eight atoms per unit cell, while the rhombohedral modification of GaSe has twelve atoms per unit cell, with C_{3v} point group symmetry.

G. B. Wright
A. Mooradian

4. The Raman Spectrum of Trigonal Selenium

The Raman spectrum of trigonal selenium has been observed using a 1.06 micron $YAG:Nd^{3+}$ laser. The D_3 point group symmetry predicts a singly degenerate A_1 and two doubly degenerate A_3 Raman active optical modes, as well as a Raman inactive A_2 optical mode. We observe three strong first order lines which we identify as an A_3 mode at $142.9\,cm^{-1}$, and an A_1 and A_3 mode at 233.7 and $237.0\,cm^{-1}$, respectively. This ordering is very similar to that calculated by Hulin[42] for tellurium using elastic constants and a simple force model. Second order lines are observed at 457, 438, 273, 206, 183, and $104\,cm^{-1}$

A. Mooradian
G. B. Wright

5. Interstellar OH Maser

A Physical Review Letter entitled "Maser Model for Interstellar OH Microwave Emission" appeared in the August 10th issue. In this letter, we describe a model of ultraviolet pumping, microwave saturation, and nonlinear interaction of propagating modes. The nearly-circular polarization observed was attributed to nonlinear mode suppression. More detailed computer calculations by P. H. Trent are almost complete for the self-consistent populations in the OH hyperfine-split Λ-doublet levels under somewhat directional UV pumping, taking into account selective absorption in the OH cloud. Also, the effect of microwave saturation on mode suppression is being further explored, both analytically and on the TX-2 computer.

M. M. Litvak   M. L. Meeks (Group 31)
A. L. McWhorter   H. J. Zeiger

REFERENCES

1. See for example, <u>Proceedings on the International Colloquium on Optical Properties and Electronic Structure of Metals and Alloys, Paris 1965</u> (N. Holland Publishing Company, Amsterdam, 1966); H. Ehrenreich, p. 109; C.N. Berglund, p. 285; W.E. Spicer, p. 296.

2. M. Garfinkel, J.J. Tiemann and W.E. Engeler, Phys. Rev. 148, 695 (1966).

3. B.R. Cooper, H. Ehrenreich and H.R. Philipp, Phys. Rev. 138, A494 (1965) and other references cited therein.

4. F. Herman and S. Skillman, <u>Atomic Structure Calculations</u> (Prentice-Hall, New Jersey, 1963).

5. C.N. Berglund and W.E. Spicer. Phys. Rev. 136, A1030, A1044 (1965); A.J. Blodgett and W.E. Spicer, Phys. Rev. 146, 390 (1966).

6. M.G. Priestley, L. Windmiller, J.B. Ketterson and Y. Eckstein, private communication.

7. P.J. Lin and L.M. Falicov, Phys. Rev. 142, 441 (1966).

8. G.W. Ludwig, Phys. Rev. 137, A1520 (1965).

9. W.E. Krag, H.J. Zeiger, Phys. Rev. Letters 8, 485 (1962).

10. W.E. Krag, W.H. Kleiner, H.J. Zeiger and S. Fischler, Bull. Am. Phys. Soc. 9, 705 (1964).

11. D.M. Larsen and E.J. Johnson, Proc. Intern. Conf. Semicond., Kyoto, Japan, 1966.

12. E.J. Johnson and D.M. Larsen, Phys. Rev. Letters 16, 655 (1966).

13. Solid State Research Report, Lincoln Laboratory, M.1.T. (1965:2) p. 63, DDC 624611.

14. R. Piotrzkowski, S. Porowski, Z. Dziuba, J. Ginter, W. Girat and L. Sosnowski, Phys. Stat. Sol. 8 K135 (1965).

15. C.R. Whitsett, Phys. Rev. 138, A829 (1965).

16. E.O. Kane, J. Phys. Chem. Solids 1, 249 (1957).

17. M. Cardona, J. Phys. Chem. Solids 24, 1543 (1963).

18. R.L. Bell and K.T. Rodgers, to be published in Phys. Rev.

19. B. Booth and A.W. Ewald, private communication.

20. P.N. Argyres, Phys. Rev. 99, 1641 (1955); Westinghouse Research Report 60-94760-2-R6 (1955).

21. B. Lax and J.G. Mavroides, <u>Advances in Solid State Physics</u> (edited by F. Seitz and D. Turnbull, vol. 11, Academic Press, New York, 1960).

22. M.H. Cohen and E.I. Blount, Phil. Mag. 5, 115 (1960).

23. P.A. Wolff, J. Phys. Chem. Solids 25, 1057 (1964).

24. W.S. Boyle and A.D. Brailsford, Phys. Rev. 120, 1943 (1960).

25. W.S. Boyle and K.F. Rodgers, Phys. Rev. Letters 2, 338 (1959).

26. C. Nanney, Phys. Rev. 129, 109 (1963).

27. H.R. Phillip and H. Ehrenreich, Phys. Rev. 129, 1550 (1963).

28. H.E. Stanley, "High Temperature Expansions for the Classical Heisenberg Model. 1. Spin Correlation Function," from Ph. D. Thesis entitled "Critical Phenomena in Heisenberg Models of Magnetism," Physics Department, Harvard University, 1967.

29. G.S. Rushbrooke and P.J. Wood, Mol. Phys. 1, 257 (1958).

30. G.A. Baker, H.E. Gilbert, J. Eve and G.S. Rushbrooke, Phys. Letters 20, 146 (1966).

31. H.E. Stanley and T.A. Kaplan, Phys. Rev. Letters 16, 981 (1966).

32. H.E. Stanley and T.A. Kaplan, Phys. Rev. Letters 17, 913 (1966).

33. P.J. Wood and G.S. Rushbrooke, Phys. Rev. Letters 17, 307 (1966).

34. C. Domb, Adv. Physics $\underline{9}$, 330 (1960), Appendix III.

35. H.E. Stanley and T.A. Kaplan, "On the Possible Phase Transition in Two-Dimensional Heisenberg Models," J. Appl. Phys. $\underline{38}$ (1967).

36. H.E. Stanley and T.A. Kaplan, "Dependence of Critical Properties Upon Spin and Lattice," J. Appl. Phys. (to be published).

37. G. Heller and H.A. Kramers, Proc. Roy. Acad. Amsterdam $\underline{37}$, 378 (1934).

38. P.N. Argyres and E.S. Kirkpatrick, Annals of Physics (to appear).

39. See, e.g., D.E. McCumber, Rev. Mod. Phys. $\underline{38}$, 494 (1966), where all earlier references are given.

40. S.V. Krivokhizha, D.I. Mash, V.V. Morozov, V.S. Starunov and I.L. Fabelinskii, JETP Letters $\underline{3}$, 245 (1966).

41. T. Ito and H. Takuma, in Physics of Quantum Electronics (McGraw-Hill, New York, 1966) pp. 200-206.

42. M. Hulin, Ann. Phys. $\underline{8}$, 647 (1963).

DOCUMENT CONTROL DATA - R&D

(Security classification of title, body of abstract and indexing annotation must be entered when the overall report is classified)

1. ORIGINATING ACTIVITY (Corporate author)	2a. REPORT SECURITY CLASSIFICATION
Lincoln Laboratory, M.I.T.	Unclassified
	2b. GROUP None

3. REPORT TITLE

Solid State Research

4. DESCRIPTIVE NOTES *(Type of report and inclusive dates)*

Quarterly Technical Summary — 1 August through 31 October 1966

5. AUTHOR(S) *(Last name, first name, initial)*

McWhorter, Alan L.

6. REPORT DATE	7a. TOTAL NO. OF PAGES	7b. NO. OF REFS
15 November 1966	80	112

8a. CONTRACT OR GRANT NO. AF 19(628)-5167	9a. ORIGINATOR'S REPORT NUMBER(S)
b. PROJECT NO. 649L	Solid State Research (1966:4)
c.	9b. OTHER REPORT NO(S) *(Any other numbers that may be assigned this report)*
d.	ESD-TR-66-566

10. AVAILABILITY/LIMITATION NOTICES

Distribution of this document is unlimited.

11. SUPPLEMENTARY NOTES	12. SPONSORING MILITARY ACTIVITY
None	Air Force Systems Command, USAF

13. ABSTRACT

This report covers in detail the solid state research work at Lincoln Laboratory for the period 1 August through 31 October 1966. The topics covered are Solid State Device Research, Optical Techniques and Devices, Materials Research, and Physics of Solids.

14. KEY WORDS

electron beam pumping	optical pumping	infrared	electroluminescence
solid state devices	impurity states	photoelectron	magnetoreflection
solid state physics	optical techniques	electronic band structure	magnetospectroscopy
laser research	and devices	magnetoabsorption	magnetoplasma
materials research	cathodoluminescence	microwave phonon	stimulated Raman scattering
hypersonic waves	magnetism	optical absorption	